Improvized photoluminescence of tin antimonide alloy

By

Muthuselvi.K

(14PPH009)

Dissertation submitted to

Avinashilingam Institute for Home Science and Higher Education for Women,

Coimbatore - 641 043

In partial fulfilment of the requirements for the degree of

Master of Science in Physics

April,2016

Improvized photoluminescence of tin antimonide alloy

By

Muthuselvi.k

(14PPH009)

Dissertation submitted to

Avinashilingam Institute for Home Science and Higher Education for Women,

Coimbatore - 641 043

In partial fulfilment of the requirements for the degree of

Master of Science in Physics

April,2016

CERTIFIED AS A BONAFIDE RESEARCH WORK

29/4/16

Signature of the Head of the Department

29/04/16

Signature of the Guide

ACKNOWLEDGEMENT

ACKNOWLEDGEMENT

I owe my sincere thanks to **Lord Almighty** and **My Lovable Parents** without whom I would have been nothing and showering their generous blessings upon me in all endeavors.

I wish to express my profound sense of gratitude to**Dr.P.R.Krishnakumar,**Ph.D**.** Chancellor, Avinashilingam Institute for Home Science and Higher Education for Women, Coimbatore, for providing the facilities to conduct this study.

I extend my thanks to **Hon.Col.Dr.(Tmt.)PremavathyVijayan,M.Sc., M.Ed., Dip.Spl.Edn., M.Phil., Ph.D,** Vice Chancellor (i/c), Avinashilingam Institute for Home Science and Higher Education for Women, Coimbatore, for providing flamboyant help towards the completion of the study.

I record my deep sense of gratitude and indebtedness to, **Dr. (Tmt.) A.Venmathi,** M.Sc, Dip.Ed, M.Phil, Ph.D. Registrar (i/c), Avinashilingam Institute for Home Science and Higher Education for Women, Coimbatore, for providing adequate help for the study.

I place on record my heartfelt thanks to **Hon.Col.Dr.(Tmt.) SarojaPrabakaran,** M.A.,Dip.Ed.,Ph.D.,Former Vice Chancellor, The Director, Hall of Residence, Avinashilingam Educational Trust Institutions Hostel, Coimbatore, for extending all possible help towards the completion of the study.

I gratefully record my sincere thanks to **Dr. (Tmt.) A. Parvathi**, M.Sc.,Dip. Ed., M.Phil., Ph.D., Dean, Faculty of Science, Avinashilingam Institute for Home Science and Higher Education for Women, Coimbatore, for timely help rendered throughout the course.

I would like to express my genial gratitude to **Dr.(Tmt.) J.Shanthi,** M.Sc., M.Phil., Ph.D., Associate Professor, Department of Physics, Avinashilingam Institute for Home Science and Higher Education for Women, Coimbatore, for her encouragement and generous help which was of great value.

I express my heartiest thanks to my guide **Dr. (Tmt.) B.Nalini,** M.Sc., Ph.D., M.S (Edu.Mgt.), STA Fellow, AIST Fellow (Japan), Assistant Professor, Department of Physics, Avinashilingam Institute for Home Science and Higher Education for Women, Coimbatore, for her inspiring guidance, meticulous care, patience, help, encouragement, motivation, and skillful and expert suggestions in completion of this work.

I sincerely thank **all the staff members** of the Department of Physics, Avinashilingam Institute for Home Science and Higher Education for Women, Coimbatore, for their help and support.

I also wish to thank **Dr.N.Shanthi**, **Assistant Professorand all staff members**, Department of Biochemistry, biotechnology and bioinformatics, Avinashilingam Institute for Home Science and Higher Education for Women, Coimbatore, for their valuable help in completion of my project.

I would like to express my special thanks to **my friends** and all **my well wishers**for their constant encouragement, support and help in carrying out this work successfully.

MUTHUSELVI.K

CONTENT

CONTENT

LIST OF FIGURES

LIST OF TABLES

INTRODUCTION

CHAPTER-I

INTRODUCTION

1.1 Introduction

Tin Antimony is one of numerous metal alloys sold by American Elements under the trade name AE Alloy. Generally, available in most volumes AE Alloys are available as bar, ingot, ribbon, wire, shot, sheet, and foil. Ultra high purity and high purity forms also include metal powder, submicron powder and nanoscale, targets for thin film deposition, and pellets for chemical vapor deposition (CVD) and physical vapor deposition (PVD) applications. American Elements produces to many standard grades when applicable, including Mil Spec (military grade); ACS, Reagent and Technical Grade; Food, Agricultural and Pharmaceutical Grade; Optical Grade, USP and EP/BP (European Pharmacopoeia/British Pharmacopoeia) and follows applicable ASTM testing standards. Let us discuss this individually.

.Tin (Sn) is a chemical element with the symbol Sn and atomic number 50. It is a main group metal of group 14 in the periodic table. Tin is the 49th most abundant element and has with a 10 stable isotopes, the largest number of stable isotopes in the periodic table. It is a soft, silvery white metal with a bluish tinge, known to the ancients in bronze,an alloy with copper,malleable other metal that is not easily oxidized in obtained chiefly from the mineral cassiterite where it occurs as tin dioxide, SnO_2. A molecules with permanent magnetic moments are called paramagnetic .Although paramagnetic substances like oxygen,tin, aluminium, and copper sulphate are attracted to a magnet then the effect is almost as feeble as diamagnetism.

Fig 1.1: Photograph of cassiterite, the mainore of tin.

1.2Discovery of tin

The first alloy used on a large scale since 3000 BC was bronze, an alloy of tin and copper. After 600 BC, the pure metallic tin were produced. Pewter, which is an alloy of 85-90% tin with the remainder commonly consisting of copper, antimony and lead, was used for flatware from the Bronze Age until the 20th century. In modern times, tin is used in many alloys, most notably tin/lead soft solders, which are typically 60% or more tin.

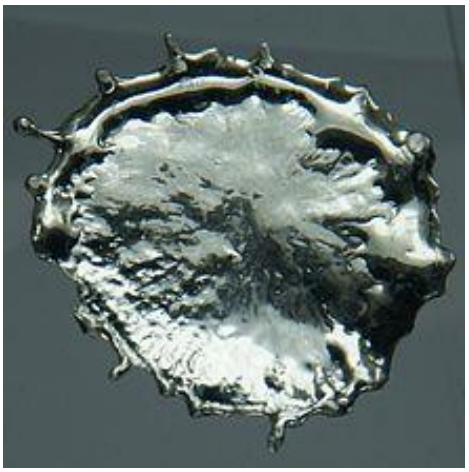

Fig 1.2: Droplet of Molten solidified tin

1.2.1 Applications

- **Tin** is used as a coating on the surface of other metals to prevent corrosion.
- Typical and custom packaging is available. Primary applications include bearing assembly, ballast, casting, step soldering, and radiation shielding.
- Another large application for tin is corrosion-resistant tin plating of steel. Because of its low toxicity, tin-plated metal was used for food packaging as tin cans, which are now made mostly of steel, even though the name is kept in English.
- **Hot Dip Coatings.** Coating of steel with lead-tin alloys produces a material called tern plate. It is easily formed and easily soldered and is used as a roofing and weather sealing material and in construction of automotive gasoline tanks, signs, radiator header tanks, brackets, chassis and covers for electronic equipment and sheathing for cable and pipe. Hot dip tin coatings are used on wire for component leads as well as food handling and processing equipment.

1.2.2 Solder

- **Tin in Alloys:** Solders account for the second largest use of tin (after tinplate). Tin is an important constituent in solders because it wets and adheres to many common base metals at temperatures considerably below their melting points.Tin is alloyed with lead to produce solders with melting points lower than those of either tin or lead. Small amounts of various metals, notably antimony and silver, are added to tin-lead solders to increase their strength. These solders can be used for joints subjected to high or even subzero service temperatures. Both solder compositions and applications of joining by soldering are many and varied.
- Commercially pure tin is used for soldering side seams of cans for special food products and aerosol sprays. The electronics and electrical industries employ solders containing 40 to 70% tin, which provide strong and reliable joints under a variety of environmental conditions. General-purpose solders (50Sn-50Pb and 40Sn-60Pb) are used for light engineering applications, plumbing and sheet metal work. Lower-tin solders (20 to 35% Sn, remainderPb) are used in joining cable and in production of automobile radiators and heat exchangers.
- In 2006, about half of tin produced was used in solder. The rest was divided between tin plating, tin chemicals, brass and bronze, and niche uses.

Fig 1.3:A coil of lead-free solder wire

- Tin has long been used as a solder in the form of an alloy with lead, tin accounting for 5 to 70% w/w. Tin forms a eutectic mixture with lead containing 63% tin and 37% lead. Such solders are primarily used for joining pipes or electric circuits. Since the European Union Waste Electrical and Electronic Equipment Directive (WEEE Directive) and Restriction of Hazardous Substances Directive came into effect on 1 July 2006, the use of lead in such alloys has decreased. Replacing lead has many

problems, including a higher melting point, and the formation of tin whiskers causing electrical problems.

- Tin pest can occur in lead-free solders, leading to loss of the soldered joint. Replacement alloys are rapidly being found, although problems of joint integrity remain.
- **Copper Alloys.** Copper-tin bronzes were some of the first alloys used by man, and these alloys continue to be used for structural and decorative purposes.
- **Dental alloys** for making amalgams contain silver, tin, mercury, and some copper and zinc. The copper increases hardness and strength and the zinc acts as a scavenger during alloy manufacture, protecting major constituents from oxidation.
- **Battery-grid Alloys.** Lead-calcium-tin alloys have been developed for storage-battery grids largely as replacements for antimonies lead alloys.
- Low-tin aluminum-base alloys (5 to 7% Sn) containing small amounts of strengthening elements, such as copper and nickel, are often used for connecting rods and thrust bearings in high-duty engines.

1.2.3 Tin plating

- Tin bonds readily to iron and is used for coating lead, zinc and steel to prevent corrosion. Tin-plated steel containers are widely used for food preservation, and this forms a large part of the market for metallic tin. A tinplate canister for preserving food was first manufactured in London in 1812.
- The light of a candle shining through the pierced design creates a decorative light pattern in the room where it sits.

Fig 1.4:**Candlestick in tin.**

1.3 Antimony

Antimony is a chemical element with a symbol Sb and atomic number 51. Antimony was named after the Greek words anti and monosmeans “a metal not found alone.” The chemical symbol Sb, comes from the element’s historical name, stibium, discovery of Antimony was a known metal in the 17th century and was likely used even earlier.

1.3.1 Discovery and Naming

Compounds of antimony were known to ancient cultures. They have been found, for example, in the colored glazes used on beads, vases, and other glassware. But these compounds were not widely used until the Middle Ages when they became popular among alchemists. They thought that antimony could be used to convert lead into gold. It was during this period that records about the properties of antimony begin to appear.

The element was probably first named by Roman scholar Pliny (A.D. 23-79), who called it stibium. Muslim alchemist Abu Musa Jabir Ibn Hayyan (c. 721-c. 815) probably first called it antimony *anti* ("not") and *monos* ("alone"). The name comes from the fact that antimony does not occur alone in nature.

Alchemists used secret codes to write about much of their work, so modern scholars do not know a great deal about how antimony was used. The first detailed reports about antimony were published in 1707 when French chemist Nicolas Lemery (1645-1715) published his famous book, Treatise on Antimony.

1.3.2 Physical properties

Antimony is a silvery-white, shiny element that looks like a metal. It has a scaly surface and is hard and brittle like a non-metal. It can also be prepared as a black powder with a shiny brilliance to it. The melting point of antimony is 630°C (1,170°F) and its boiling point is 1,635°C (2,980°F). It is a relatively soft material that can be scratched by glass. Its density is 6.68 grams per cubic centimeter. A metalloid is an element that has characteristics of both metals and non-metals.

1.3.3 Chemical properties

Antimony is a moderately active element. It does not combine with oxygen in the air at room temperature. It also does not react with cold water or with most cold acids. It does dissolve in some hot acids, however, and in aqua regia. Aqua regia is a mixture of hydrochloric and nitric acids. It often reacts with materials that do not react with either acid separately.

Isotopes

Isotope	**Half Life**
Sb-117	2.8 hours
Sb-119	38.1 hours
Sb-120	15.89 minutes
Sb-121	Stable
Sb-122	2.7 days
Sb-123	Stable
Sb-124	60.2 days
Sb-125	2.75 years
Sb-126	12.4 days
Sb-126m	19.0 minutes
Sb-127	3.84 days
Sb-129	4.4 hours

1.3.4 Occurrence in nature

Antimony is rarely found in its native (as an element) state. Instead, it usually occurs as a compound. The most common minerals of antimony are stibnite, tetrahedrite, bournonite, boulangerite, and jamesonite. In most of these minerals, antimony is combined with sulfur to produce some form of antimony sulfide (Sb_2S_3).

The largest producers of antimony are China, Russia, Bolivia, South Africa, and Kyrgyzstan. The abundance of antimony is estimated to be about 0.2 parts per million, placing it in the bottom fifth among the chemical elements found in the Earth's crust. It is more abundant than silver or mercury, but less abundant than iodine.

About 20 radioactive isotopes of antimony are also known. A radioactive isotope is one that breaks apart and gives off some form of radiation. Radioactive isotopes are produced when very small particles are fired at atoms. These particles stick in the atoms and make them radioactive.

1.3.5 Extraction

Antimony can be recovered from stibnite with hot iron. About half the antimony produced in the United States is recycled from old lead storage batteries used in cars and trucks.

1.3.6 Applications

- Antimony is used metallurgical as an additive element since the physical properties of the element are not suitable for engineering applications. Its most important use is as an alloying constituent for lead and lead-base alloys to impart hardness and stiffness, and to improve the corrosion resistance.
- It is also used as an alloying ingredient for tin alloys to produce pewter, and tin-basebabbits for bearing metal applications. The element is also used in cable covering, castings, solder, etc.
- Important III-V compounds such as InSb, GaSb are made from high purity antimony. These compounds may be used as infrared detectors, diodes and Hall effect devices. The compound in this group with the biggest technological importance is InSb.
- Antimony is alloyed with lead to increase lead's durability. Antimony alloys are also used in batteries, low friction metals, type metal andcable sheathing, among other products. Antimony compounds are used to make flame-proofing materials, paints, ceramic enamels, glass and pottery.

- Antimony compounds have been used by humans for centuries. Women of ancient Egypt used stibic stone, antimony sulfide, (Sb_2S_3), to darken their eyes. Antimony was also used in making colored glazes for beads and glassware. The chemical symbol for antimony was taken from the ancient name for the element, stibium. Not recognized as a chemical element until the Middle Ages, antimony became a common material used by alchemists.

1.3.7 Health Effects:

- Antimony and its compounds are dangerous to human health. In low levels, these materials can irritate the eyes and lungs. They may also cause stomach pain, diarrhea, vomiting, and stomach ulcers. At higher doses, antimony and its compounds can cause lung, heart, liver, and kidney damage. At very high doses, they can cause death.

1.4 Experimental study of SnSb alloy

Tin antimony sulphide ($S_nS_bS_5$) thin film was deposited by common vacuum thermal evaporator by two sources technique. Initial materials prepared were tin sulphide (SnS) and antimony sulphide (Sb_2S_3). Tin sulphide was manufactured from tin and sulphur powder , which were grinded in pestle and mortar and annealed in quartz ampoule containing argon gas for 24 h at 600°C(Sb_2S_3), Sb_2S_3 of analytical grade was obtained from sigma Aldrich (Kurt J. Lesker) with 99.99% purity. The powdered SnS and Sb_2S_2, placed in Al_2O_3 crucibles, were evaporated simultaneously in a vacuum chamber in order to deposit thin films on glass substrates. The pressure of the chamber was sustained at approximately 10^{-5}torr. The prepared films were annealed at different temperatures such as 125°C, 175°C and 250°C. The structural characterization of the films was performed by means of conventional JDX3532 diffractometer with Cu Kα radiation (λ=1.54Å). The optical absorption, transmission, band gap and film thickness data were obtained by the modelled ellipsometric data by using Sentech variable angle spectroscopic ellipsometer (VASE). The thickness of the film was measured as 1400 nm. The type of conductivity of the sample was examined by using hot Point probe.

Doping

Doping is the process of adding impurities to intrinsic semiconductors to alter their properties. Normally, Trivalent and Pentavalentelementsare used to dope Silicon and

Germanium. When a intrinsic semiconductor is doped with Trivalent impurity it becomes a P-Type semiconductor.

The lanthanide series of chemical elements comprises the fifteen metallicchemical elements with atomic numbers 57 through 71, from lanthanum through lutetium. These fifteen lanthanide elements, along with the chemically similar elements scandium and yttrium, are often collectively known as the rare earth elements.

Lanthanide elements and their compounds have many uses but the quantities consumed are relatively small in comparison to other elements. About 15000 ton/year of the lanthanides are consumed as catalysts and in the production of glasses. This 15000 tons corresponds to about 85% of the lanthanide production. From the perspective of value, however, applications in phosphors and magnets are more important.

1.5 Dysprosium chloride

Dysprosium is a chemical element with the symbol Dy and atomic number 66. It is a rare earth element with a metallic silver luster. Dysprosium is never found in nature as a free element, though it is found in various minerals, such as xenotime. Naturally occurring dysprosium is composed of seven isotopes, the most abundant of which is ^{164}Dy. Dysprosium was first identified in 1886 by Paul EmileLecoq de Boisbaudran.

Dysprosium is used, in conjunction with vanadium and other elements, in making laser materials and commercial lighting. Because of dysprosium's high thermal-neutron absorption cross-section, dysprosium-oxide–nickel cermets are used in neutron-absorbing control rods in nuclear reactors. Dysprosium carbonate,$Dy_2(CO_3)_3$, and dysprosium sulfate, $Dy_2(SO_4)_3$, result from similar reactions.Most dysprosium compounds are soluble in water, though dysprosium carbonate tetrahydrate ($Dy_2(CO_3)_3{\cdot}4H_2O$) and dysprosium oxalate decahydrate ($Dy_2(C_2O_4)_3{\cdot}10H_2O$) are both insoluble in water.Two of the most abundant dysprosium carbonates, tengerite-(Dy) ($Dy_2(CO_3)_3{\cdot}2–3H_2O$) and kozoite-(Dy) ($DyCO_3(OH)$) are known to form via a poorly ordered (amorphous) precursor phase with a formula of $Dy_2(CO_3)_3{\cdot}4H_2O$.

Isotopes

Naturally occurring dysprosium is composed of seven isotopes there are ^{156}Dy, ^{158}Dy, ^{160}Dy, ^{161}Dy, ^{162}Dy, ^{163}Dy, and ^{164}Dy. These are all considered stable,

although ^{156}Dy decays by alpha decay with a half-life of over 1×10^{18} years. Of the naturally occurring isotopes, ^{164}Dy is the most abundant at 28%, followed by ^{162}Dy at 26%. The least abundant is ^{156}Dy at 0.06%.

PRECAUTIONS

Soluble dysprosium salts, such as dysprosium chloride and dysprosium nitrate, are mildly toxic when ingested. The insoluble salts, however, are non-toxic. Based on the toxicity of dysprosium chloride to mice, it is estimated that the ingestion of 500 grams or more could be fatal to a human.

A radioactive isotope is one that is unstable, gives off radiation, and breaks down to form a new isotope. Of these eight isotopes, only one, dysprosium-166, has much commercial importance

LUMINESCENCE MECHANISMS

Luminescence is a process that corresponds to the emission of electromagnetic radiation beyond thermal equilibrium**.**

Inorganic luminescent materials – Requirements for high efficiency

• Strong absorption
• Highly crystalline particles, low defect density
• High purity (99.99% or higher)
• Homogeneous distribution of activator and sensitizer ions
• Low photon frequencies.

1.5.4 Objective of the Present Work

We have analysed about the SnSb alloy as prospective host lattice,also studied about the rare earth element dysprosium and its properties. The alloys in nanoparticle range will be very useful in emission or phosphorescence behaviour, the rare earths would be good additive to improve the emission profile of nanomaterial. Hence the objective is to study the luminescence profile of tin antimony doped with dysprosium (rare earth).

REFERENCES

1.) J. Reichman, Handbook of Optical Filters for Fluorescence Microscopy (Chroma Technology, Brattleboro,(2010)

2.) C. Ronda,Luminescence From Theory to Applications (Wiley-VCH, New York, 2008)

3). I. Parreu, J.J. Carvajal, X. Solans, F. Díaz, M. Aguiló, Chem. Mater. 18, 221 (2006)

4). I. Parreu, R. Sole, J. Gavalda, J. Massons, F. Díaz, M. Aguilo, Chem. Mater. 15, 5059 (2003)

5.) P. Bamfield, M.G. Hutchings, Chromic Phenomena Technological Applications of Colour Chemistry, 2nd edn. (The Royal Society of Chemistry, Cambridge, 2010)

6) L. Strekowski,Heterocyclic Polymethine Dyes, Topics in Heterocyclic Chemistry (Springer, Berlin, 2008), p-14

7) P. Goldberg,Luminescence of Inorganic Solids(Academy Press, New York, 1966)

8) E. Nakazawa, S. Shionoya, J. Phys. Soc. Jpn. 28, 1260 (1970)

9)D. Jia,W. Jia, D.R. Evans,W.M. Dennos, H. Liu, J. Zhu,W.M. Yen, J. App. Phys. 88(6), 3402
(2000)

10) H. Agura, A. Suzuki, T. Matsushita, T. Aoki, and M. Okuda,
Thin Solid Films. 445- 263 (2003) [DOI: 10.1016/S0040-6090(03)01158-1].

11) T. Karasawa, and Y. Miyata, Thin Solid Films. 223- 135 (1993)

12)Elumalai, P., Atkins, P., de Paula, J. Atkins' Physical Chemistry, Oxford University Press, 2002. ISBN 0-19-879285-9

REVIEW OF LITERATURE

CHAPTER-II

REVIEW OF LITERATURE

1) **B.L.Chen *et al.*,(2004)** have discussed about the influence of Sb on the soldering reaction and growth kinetics of Intermetallic compound (IMC) in Sn–3.5Ag–0.7 Cu–$_x$Sb (x = 0, 0.5,1.0, and 1.5) lead-free solder joints were investigated in this study. Scanning electron microscope (SEM) is used to observe microstructure evolution of solder joint and to estimate the thickness and the grain size of the intermetallic layers. IMC phases are identified by energy dispersive X-ray (EDX) and X-ray diffractometer (XRD). Results show that some of the Sb powders are dissolved in the h-Sn matrix (Sn-rich phase), some of them participate in the form of Ag_3(Sn, Sb), and the rest dissolves in the CU_6Sn_5 IMC layer. Both thickness and grain size of IMC decrease when Sb is added. The growth exponents for both IMC layer and grains are determined by curve-fitting. The results reveal that Sn–3.5Ag–0.7Cu with about 1.0 wt.% Sb solder system exhibits the smallest growth rate and gives the most prominent effect in retarding IMC growth and refining IMC grain size. Based on the thermodynamic and phase diagram analysis, Sb has higher affinity to Sn element, and it will reduce the activity of Sn by forming SnSb compound, resulting in a decreased driving force for Cu–Sn IMC formation. A heterogeneous nucleation effect for retarding the IMC growth due to Sb addition is proposed.

2) **MUSTAFA KAMAL *et al.*,(2006)** have studied about the influence of ternary and quaternary alloying elements (Pb, Cd, Cu or Cu–Pb and Cu–Cd) on structural, electrical, hardness and other mechanical properties of Sn–Sb alloys (using an X-ray diffractometer and optical microscope, the double bridge method, Vickers hardness tester and the dynamic resonance method) to produce the best alloy for bearing applications. Adding Cu or Pb to Sn–Sb alloys improves their bearing properties, such as the mechanical properties (elastic modulus, internal friction, hardness and fracture strain) and thermal conductivity. Also, adding Cu, Pb or Cu–Pb to Sn–Sb alloys makes them excellent in their bearing applications and environmental hazards when compared with the $Pb_{88}Sn_{10}Cu_2$ alloy for automotive applications (FIAT Normalizzazione) and the lead-based Babbitt bearing alloy.

3) **Hailei Zhao *et al.*,(2008**) have studied the Micro-sized Sb/SnSb composite synthesized by carbo thermal reduction shows a high-specific capacity (ca. 650 mAh/g), a low initial irreversible capacity loss (∼14%) and a good cycling stability, which are described to the lower specific surface area and the polycrystalline feature of the synthesized Sb/SnSb particles. The large amount of grain-boundaries inside the Sb/SnSb particles can relieve the mechanical stress, originated from the big volume changes upon lithiation and delithiation, by grain-boundary slipping, and thus maintain the structure stability of electrode. The electrode reaction process is characterized by cycling voltammetry and AC impedance techniques. The results indicate that the some local cracking of the SEI film may occur due to the large volume changes of active materials and the new film formation takes place. This will not only consume some lithium and thus produce the irreversible capacity loss during cycling process, but also result in decreased SEI film resistance and charge transfer resistance.
4) **Qianlei Jianga *et al.*,(2011)** have discussed about the preparation of Sn–Sb–Cu anodes started with galvanostatic electrochemically depositing antimony and tin sequentially on the substrate of copper foil collector. Sn–Sb and Cu–Sb alloys are formed when heated. The SEM analysis showed that the crystalline grains become bigger and the surface of the Sn–Sb–Cu anode becomes more denser after annealing. The energy dispersive spectroscopy (EDS) and X-ray diffraction (XRD) analysis showed the antimony, tin and copper are alloyed to form SnSb and Cu_2Sb after heat treatment. The X-ray photoelectron spectroscopy(XPS) analysis showed the surface of the Sn–Sb–Cu electrode is covered by a thin oxide layer. Electrochemical measurements showed that the annealed Sn–Sb–Cu anode has high reversible capacity and good capacity retention. It exhibited a reversible capacity of about 962 mAh/g in the initial cycle, which still remained 715 mAh/g after 30 cycles.
5) **Hao Xu *et al.*,(2011)** have employed the new spin-coating method coupling with high thermal decomposition, to prepare the tin-antimony (Sn–Sb) oxide electrode. The character of the spin-coating electrode is compared with the dip-coating electrode through X-ray diffraction (XRD), scanning electron microscopy (SEM), accelerated life test, cyclic voltammetry, and electrolytic degradability. The results showed that the spin-coating electrode had a better defined crystal form, a smoother and more compact surface than that of the dip-coating electrode. Service time of the spin-coating electrode is determined to be longer than 15 h, and it is less than 2 min for the dip-

coating electrode. Electrochemical characterization analysis showed that the electrolytic degradability of the spin coating electrode is better than that of the dip-coating electrode.

6) **Sinn-wen Chen *et al.*,(2011)** have discussed about the ternary Sn–Sb–Cu alloys. The primary solidification phases, the phase transformation temperatures, and the equilibrium phases at 250^0C are experimentally determined. The liquidus projection and the 250^0 C phase equilibria isothermal section of the Sn–Sb–Cu system are proposed based on the experimental results and the phase diagrams of the three constituent binary systems. Using the CALPHAD approach, thermodynamic modelling of the Sn–Sb–Cu ternary system is carried out based on the experimental information determined in this study and those in the literatures, together with the developed thermodynamic models of the three constituent binary systems. The liquidus projection and the isothermal sections are then calculated using the models developed in this study and the results are in good agreement with experimental determinations.

7) **Nisar Ali *et al.*,(2011)** have studied about the thin films of $SnSb_2S_4$ prepared on glass substrate by using thermal evaporation techniques. The films are annealed in argon gas at low pressure in sealed glass ampoules at 85^0C, 150^0C, 275^0C and 325^0C .XRD of the films reveal that the low temperature annealed films are polycrystalline while the as deposited films and high annealed films are in amorphous states. There is no adequate variation in the photoconductivity response of the amorphous and crystalline phases. The transmittance of the films is low and having no transmittance below 740 nm. The band gap calculated by ellipsometry technique is in the range of 1.82–3.1 eV. The films have n-type conductivity but the film annealed at 325^0C show p-type conductivity.

8) **Yu Muto *et al.*, (2011)** have discussed the SnO_2 films doped with Sb (ATO) that are deposited both on the unheated glass substrates and on glass substrates that had been heated at 200 °C by reactive sputtering of an Sb–Sn alloy target with a plasma control unit (PCU) and mid-frequency (mf, 50 kHz) unipolar pulsing. The PCU feedback system monitors the oxidation states of target surface by detecting the sputtering cathode voltage (impedance control method). The mf pulse wave is approximately square-shaped; this helps to reduce arcing on the target when high power density is applied on the cathode. In case of the ATO depositions on the heated substrate at 200°C in the “transition region” of reactive sputtering, the deposition rate is 280

nm/min, the lowest resistivity of the ATO filmsis 4.6×10−3Ω cm and the optical transmittance was over 80% in the visible region of light.

9) **Leszek Zaraska *et al.*, (2012)** have studied about theAntimony nanowires with diameters ranging from 35 nm to 320 nm that are successfully prepared by simple, galvano static electro deposition inside the pores of anodic alumina membranes from a citrate based electrolyte. The use of the potassium antimonyl tartrate electrolyte for electrodeposition results in the formation of Sb/Sb_2O_3 nanowires. The structural features of the nanowire arrays are investigated by FE-SEM, and the nanowire composition is confirmed by ED and XRD measurements. A distinct peak at about 27.5 in the XRD pattern recorded for nanowires formed in the tartrate electrolyte is attributed to the presence of co-deposited Sb_2O_3. Three types of dense arrays of Sn–SnSb nanowires with diameters ranging from 82 nm to 325 nm are also synthesized by DC galvanostatic electro deposition into the anodic aluminum oxide (AAO) membranes for the first time. Only Sn and SnSb peaks appeared in the XRD pattern and both phases seem to have a relatively high degree of crystallinity. The influence of current density applied during electrodeposition on the composition of nanowires was investigated. It is found that the Sb content in fabricated nanowires decreases with increasing the current density. The diameters of all synthesized nanowires roughly correspond to the dimensions of the nano channels of AAO templates used for electrodeposition

10) **LingXin Kong *et al.*,(2013)** have discussed in this paper, are the molecular interaction volume model (MIVM) has been used for a calculation of the activities of components of Pb-Sn-Sb ternary alloy system. The separation coefficients of the related binary alloys Sn-Pb and Sn-Sb and the vapour-liquid phase equilibrium of the Pb-Sn-Sb alloy system are also calculated by using the MIVM. Experiments for the separation of the Pb-Sn-Sb ternary alloy are carried out for the proper interpretation of the results of the model. The predicted data are in good agreement with the experimental results, which indicates that MIVM is reliable and convenient since it has certain physical meaning from the view point of statistical thermodynamics and requires only two infinite dilute activity coefficients for each sub-binary system.

11) **Y. Kaygisiz *et al.*, (2013)** have studied about the equilibrated grain boundary groove shapes of solid Sn_3Sb_2 in equilibrium with the Sn–Sb peritectic liquid have been observed from quenched sample with a radial heat flow apparatus. The Gibbs–Thomson coefficient, solid–liquid interfacial energy and grain boundary energy of

solid Sn_3Sb_2 have been determined from the observed grain boundary groove shapes. The variation of thermal conductivity with temperature for solid Sn_3Sb_2 and peritectic solid has been measured up to five degree below the melting temperature with a radial heat flow apparatus. The ratio of thermal conductivity of liquid phase to solid phase for Sn–7.8 at % Sb alloy at the melting temperature has also been measured with a Bridgman type growth apparatus.

12) **Laxmikanta Dua *et al*., (2013)** have studied about the Sol–gel Mn(II) doped antimony tin oxide films were developed with precursor of atomic ratio range, Sn:Sb:Mn = 68–72:23–25:9–3. The X-ray diffraction patterns depict tetragonal cassiterite phase of Sn_{O2}. Transmission electron microscopy images suggest the nanostructured form of the doped materials. The increase in crystallite size with Mn(II) concentration is reflected by the larger band gap values (4.61–4.73 eV) arising from the excitonic transitions which also respond to PL emissions. Hall effect measurements shows that the carrier concentration increases but mobility decreases for Mn(II) doping. Room temperature ferromagnetism with different saturation magnetic moments (Ms) has been observed for all dopant concentrations at 3–9 %.

13) **Francisco Lopez Morales *et al.*, (2013)** have discussed about SnO_2 and Sb-doped SnO_2 particles that are synthesized using the polymeric precursor method with different Sn salt precursors: $SnCl_2 \cdot 2H_2O$, $SnCl_4 \cdot 5H_2O$, or Sn citrate. Sb_2O_3 is used as the precursor of Sb, and the molar ratio of *Sn-Sb* is held constant. FTIR and TGA/DTA are used to examine the influence of the Sn precursor on the formation and thermal decomposition of the Sn and Sn-Sb complexes. The calcination products obtained from heating the Sn and Sn-Sb complexes at 500°C in air were analysed using XRD and TEM analysis. The results revealed that the SnO_2 and Sb-doped SnO_2 formation temperatures depended on the nature of the Sn precursor. The calcination products are found to be SnO_2 and Sb-doped SnO_2 particles, which crystallized in a tetragonal cassiterite structure with a highly preferred (110) planar orientation. The Sn precursor and the presence of Sb in the SnO_2 matrix strongly influences the crystallinity and lattice parameters.

14) **Yerpude *et al.*,(2013)** have studied the Eu^{3+}, Dy^{3+} activated $SrCaAl_2O_5$ phosphor that are synthesized by the combustion method at 550°C. The prepared phosphor characterized by X-ray diffraction and photoluminescence measurements. The photoluminescence studies of the Eu^{3+} doped phosphor shows that the intensity of electric dipole transition ($^5D_0 \rightarrow {}^7F_2$) at 615 nm dominates over that of magnetic dipole

transition ($^5D_0 \rightarrow {}^7F_2$) at 596 nm under 395 nm excitation. The PL emission spectrum of Dy^{3+} ion at 350nm excitation gives an emission band at 484 nm (blue) and 575 nm (yellow). The optimum concentration of both the dopant having highest luminescence intensity is found to be 0.5 mole %. The obtained PL results indicated that the prepared phosphor is suitable as near UV excited white light-emitting diodes.

15) **Peixin Zhang *et al.*,2014*)*** have investigated about the $SnSbAg_{0.1}$ reduced graphene oxide (RGO) composite anode materials that are synthesised via chemical reduction. The structure, morphology and electrochemical performance of the synthesised materials are characterised by X-ray diffraction (XRD), scanning electron microscopy (SEM), X-ray photoelectron spectroscopy (XPS), transmission electron microscopy, Raman spectrometry, galvanostatic charge-discharge and cyclic voltammetry techniques. The large surface area, excellent conductivity and mechanical properties of the graphene reduce the agglomeration of alloy particles, buffer the stress of volume change and lower the powdering rate of particles, to enhance the inner transportation of Li^+ between the electrodes and the electrolyte. The SnSbAg0.1-10%RGO composite anode materials exhibit a better electrochemical performance and cycle life than other alloy anode composite materials, demonstrating a capacity of 605.1mAh g^{-1}after 100 cycles and an average capacity attenuation rate of 0.16% from the 2^{nd} cycle to the100^{th}cycle. The discharge capacity remain 538mAh g^{-1}after 200 cycles, retaining 74.3% of its capacity compared to the 2^{nd} cycle and therefore exhibiting an excellent electrochemical performance**.**

16) **P. Nithyadharseni *et al., (*2014)** have studied about the influence of incorporating transition metal impurities such as Fe, Co and Ni on the magnetic and electrical properties of SnSb alloy nanopowders synthesized by the reductive co-precipitation is reported. Structural elucidation of all the samples by X-ray diffraction (XRD) confirms hexagonal structure and the morphological observations through scanning electron microscope (SEM) show a minimal particle size of 20 nm for the Co substituted SnSb sample, among all the other impurity incorporated samples. Compositional confirmation of Sn, Sb, Fe, Co, and Ni was made using EDAX. The X-ray photoelectron spectroscopy (XPS) is used to investigate the surface of SnSb and the change in surface activity due to the addition of transition metal impurities. The magnetic hysteresis studies indicates that the SnSb and SnSb:Ni exhibit diamagnetic behaviour; where the Fe and Co incorporation resulted in ferromagnetic nature. The conductivity of SnSb:Fe, SnSb:Ni shows a semiconducting nature with the negative

temperature coefficient of resistance; whereas pure and Co substitution exhibit metallic behaviour with positive temperature coefficient of resistance. The switching of metallic to semiconducting regime was explained in this paper. Also an attempt has been made to correlate electrical and magnetic properties with the surface oxidation effect through XPS data.

17) **Loic Baggetto *et al.*, (2014)** have studied about the electrochemical reaction of Sb and SnSb anodes with Na results in the formation of amorphous materials. To understand the resulting phases and electrochemical capacities are studied the local order using 119Sn and 121Sb Mossbauer spectroscopies in conjunction with measurements performed on model powder compounds of Na-Sn and Na-Sb to further clarify the reactions steps. For pure Sb the sodiation starts with the formation of an amorphous phase composed of atomic environments similar to those found in NaSb, and proceeds further by the formation of crystalline Na_3Sb. The reversible reaction takes place during a large portion of the charge process. At full charge the anode material still contains a substantial fraction of Na, explaining the lack of recrystallization into crystalline Sb. The reaction of SnSb yields Na_3Sb at full discharge at higher temperatures (65^0 C and 95^0 C) while the Room temperature (RT) reaction yields amorphous compounds. The electrochemically-driven, solid-state amorphization reaction occurring at RT is governed by the simultaneous formation of Na-coordinated Sn and Sb environments, as monitored by the decrease (increase) of the 119Sn (121Sb) Mossbauer isomer shifts. Overall, the monitoring of the hyperfine parameters enables to correlate changes in Na content to the local chemical environments. Here, they have discussed about the structural properties of the products of Sb and SnSb thin films during the electrochemical reaction with Na using X-ray diffraction.

18) **Anxiang Wang *et al.*,(2014)** have studied on the molecular interaction volume model (MIVM), the vapour- liquid phase equilibrium of Sn-Sb Alloy is calculated, which is used to predict the element distribution of Sn-Sb alloy between the vapour and liquid phase during vacuum distillation. A central composite design (CCD) was used to optimize the process parameters influencing the content of Sn in liquid phase and the direct yield of Sn. The studied parameters are distillation temperature, feeding materials and soaking time. Two quadratic mathematical model equations are derived for predicting the content of Sn in liquid phase and the direct yield of Sn. The analysis of variance (ANOVA) shown that the distillation temperature was the most significant factor affecting the separation of Sn-Sb alloy. In the process optimization, while the

direct yield of Sn equal to 92%, the maximum content of Sn in liquid phase should be 99.66 wt.% under the conditions of 1531 K, 137 g and 46 min. The confirmation test values of 91.22% and 99.43 wt. % are fair agreement with the predicted data, which demonstrated that these models were very good and can be used for parameter optimization in vacuum distillation.

19) **M. A. Khan *et al.*, (2016)** have studied the tin antimony sulphide thin films are synthesized as an absorber layer for solar cells. These films are deposited by vacuum thermal evaporation on glass substrate at a pressure of 10-5 torr. The films are then annealed at different temperatures in argon atmosphere. XRD analysis reveals that both as deposited and annealed films are found to be in polycrystalline phase. The crystallinity of the films is significantly enhanced with increasing annealing temperatures. The quantum efficiency is higher in the visible and near infrared region for the annealed films whereas the quantum efficiency of as deposited film is comparatively lower. The transmittance of the annealed films is found to be decreasing with increasing temperatures. The thickness and band gap of the films are measured by ellipsometric data. The absorption coefficient of the films is significantly higher (~105cm-1), which is very important factor regarding solar conversion efficiency. Hot point probe measurements show that the films possess n-type electrical conductivity.

2.2 REFERENCES

1)B.L. Chen, G.Y. Li . Influence of Sb on IMC growth in Sn–Ag–Cu–Sb Pb-free solder joints in reflow process School of Materials Engineering, Nanyang Technological University, Thin Solid Films 462–463 (2004) 395– 401

2)Mustafa kamal, B.I. Shklovskii A.L. Efros Influence of alloying elementson structure and some physical properties of quenched sn-sb alloy ,Electronic properties of Doped semiconductor.pag 142-146.

3)Hailei Zhao, Zhiming Zhu, Chaoli Yin , Hong Guo, Dickon H.L. Ng.Electrochemical characterization of micro-sized Sb/SnSb composite anodeMaterials Chemistry and Physics 110 (2008) 201–205

4) Qianlei Jianga, Ruisheng Xueb, Mengqiu Jia, Electrochemical performance of Sn–Sb–Cu film anodes prepared bylayer-by-layer electrodeposition Applied Surface Science 258 (2012) 3854– 3858

5) Hao Xu, Wei Yan , Cheng Li Tang. A novel method to prepare metal oxide electrodeSpin-coating with thermal decomposition Chinese Chemical Letters 22 (2011) 354–357

6) Sinn-wen Chen, An-ren Zi , Wojciech Gierlotka, Ching-feng Yang, Chao-hong Wang, Shih-kang Lina,, Chia-ming Hsu Phase equilibria of Sn–Sb–Cu system Materials Chemistry and Physics 132 (2012) 703– 715

7) Nisar Ali , S.T. Hussain, M.A. Iqbal, Kyle Hutching, David Lane Structural and optoelectronic properties of antimony tin sulphide thin filmsdeposited by thermal evaporation techniques Optik 124 (2013) 4746– 4749

8) Yu Muto, Nobuto Oka , Naoki Tsukamoto , Yoshinori Iwabuchi , Hidefumi Kotsubo, Yuzo Shigesato ,Yu Muto, Nobuto Oka,Naoki Tsukamoto,Yoshinori Iwabuchi, Hidefumi Kotsubo , Yuzo Shigesato, High-rate deposition of Sb-doped SnO2 films by reactive sputtering using the impedance control method Thin Solid Films 520 (2011) 1178–1181

9) Leszek Zaraska, Elzbieta Kurowska, Grzegorz D.Sulka ,Marian Jaskuła Template-assisted fabrication of tin and antimony based nanowire arrays Applied Surface Science 258 (2012) 9718– 9722

10) LingXin Kong , Bin Yang , BaoQiang Xu, YiFu Li , DaChun Liu, YongNian Dai Application of MIVM for Pb-Sn-Sb ternary system in vacuumdistillation The National Engineering Laboratory for Vacuum Metallurgy, Kunming University of Science and Technology, Vacuum 101 (2014) 324-327

11)Y. Kayiisiz, Y.Ocak, S.Aksoz, K. Kes, lioglu, N. Maras, Thermal conductivity and interfacial energies of solid Sn3Sb2 in the Sn–Sb peritectic system Thermochimica Acta 520 (2011) 25–32

12) Laxmikanta Dua, Prasanta K. Biswas. Synthesis and characterization of nanostructured Mn(II) doped antimony-tin oxide (ATO) films on glass Applied Surface Science 280 (2013) 33– 41

13) Francisco Lopez Morales, He Shao-Bo, Wang Shi-Fa. Role of chelating agent in chemical and fluorescent properties of SnO2 nanoparticles_ Chin. Phys. B Vol. 22, No. 5 (2013)

14)A.N. Yerpude and S.J. Dhoble Trivalent rare earth activated SrCaAl2O5 phosphor for white light-emtting diode , Adv. Mat. Lett. 2013, **4**(10), 792-796

15) Peixin Zhang, Yanyi Wang, Jingwei Wang, Dongyun Zhang,Xiangzhong Ren, Qiuhua Yuan Influence of reduced graphene oxide on the morphology and electrochemical performance of $SnSbAg_{0.1}$ composite materials.Electrochimica Acta 137 (2014) 121–130.

16) P. Nithyadharseni, B. Nalini , P. Saravanan Electrical and magnetic effect of transition metals in SnSb nanoalloy.Applied Surface Science 311 (2014) 503–507

17) Loic Baggetto , Hien-Yoong Hah , Jean-Claude Jumas , Charles E. Johnson , Jacqueline A. Johnson , Jong K. Keum , Craig A. Bridges , Gabriel M. Veith.
The reaction mechanism of SnSb and Sb thin film anodes for Na-ion batteries studied by X-ray diffraction, 119Sn and 121Sb Mossbauer spectroscopies Journal of Power Sources 267 (2014) 329-336

18) Anxiang Wang Lingxin Kong, Bin Yang, Baoqiang Xu, Yifu Li Application of MIVM for phase equilibrium of Sn–Pb–Sb system invacuum distillation Fluid Phase Equilibria 364 (2014) 1– 5

19)M. A. Khan,, Azhar Ahmed, N. Ali, Tariq Iqbal, Ayaz Arif Khan, Mahboob Ullah, Muhammad Shafique Improved Optical Properties of Tin Antimony Sulphide Thin Films for PhotovoltaicsAmerican Journal of Materials Science and Engineering, 2016, Vol. 4, No. 1, 1-6

MATERIALS AND METHODS

CHAPTER III

MATERIALS AND METHODS

3.1 INTRODUCTION

This chapter describes about the experimental techniques used in the preparation and characterization of Dysprosium doped SnSb. The method of preparation used in this study is to prepare SnSb doped with dysprosium in co-precipitation technique. The various experimental techniques were used. They are Photoluminescence (PL), X-ray Diffraction (XRD), Fourier Transform Infra-Red (FTIR) and (SEM) Scanning Electron Microscope, UV Spectroscopy.

3.2 METHODS OF PREPARATION

The raw materials chosen are

- Tin chloride ($SnCl_2$)
- Antimony chloride ($SbCl_3$)
- Trisodium citrate ($Na_3C_6H_5O_7$)
- Dysprosium chloride($dyCl_3$)
- Sodium hydroxide (NaOH)
- Sodium borohydride ($NaBH_4$)

The raw materials are taken in appropriate gram molecular weights and dissolved in 50ml distilled water. The two solutions, later two in a separate solution, are stirred for 30min and 20 minutes separately and mixed to each other dropwise until precipitate forms. The precipitate thus formed is washed thoroughly with dilute HCl, Water and acetone for several times to remove residual chlorine in the precipitate.

3.3 Structural and Morphological Studies

3.3.1 X-Ray Diffraction (XRD):

X-ray Diffraction (XRD) is a powerful non-destructive technique for characterizing the crystalline material. XRD is a rapid analytical technique primarily used for phase identification of a crystalline material and can provide information on unit cell dimensions. It offers information on structures, phases, preferred crystal orientations, and other structural parameters, such as crystallinity, grain size, strain, and crystal defects. X-ray powder

diffraction is most widely used for the identification of unknown crystalline materials (e.g. minerals, inorganic compounds). Determination of unknown solids is critical to studies in geology, environmental science, material science, engineering and biology.

The prepared material is finely ground and homogenized. X-ray diffraction is the interference of a monochromatic beam of x-rays scattered at angles from each set of lattice planes in a sample. The peak intensities are determined by the specified atoms in the lattice. XRD is a fingerprint of a periodic arrangement in a material.

Principles of X-ray Diffraction:

Max von Laue, in 1912, discovered that crystalline substances act as three-dimensional diffraction gratings for X-ray wavelengths similar to the spacing of planes in a crystal lattice. X-ray diffraction is now a common technique for the study of crystalline structures and atomic spacing. X-ray Diffraction (XRD) is a very important experimental technique that has been used for a long time to study the crystal structure of solids, lattice constants and geometry identification of unknown materials.

X-ray diffraction is based on the constructive interference of monochromatic X-rays in a crystalline sample. These X-rays were generated by a cathode ray tube, filtered to produce monochromatic radiation, collimated to concentrate, and directed towards the sample. The interaction of the incident rays with the sample produces constructive interference (and a diffracted ray) when the conditions satisfy the law as,

Bragg's Law:

$$n\lambda = 2d \sin\theta$$

where n is the order of diffraction

l is the wavelength of the X ray

q is the angle between the incident ray and diffracted ray

This law relates the wavelength of electromagnetic radiation to the diffraction angle and the lattice spacing in a crystalline sample. These diffracted X-rays are then detected, processed. By scanning the sample through a range of 2θ angles, all possible diffraction directions of the lattice could be obtained due to the random orientation of the powdered material. Conversion of the diffraction peaks to d-spacing allows identification of the mineral

because each mineral has a set of unique d-spacing. Typically, this is achieved either by comparison of d-spacing with standard reference patterns or by assigning to the respective d spacing formula of various crystal structures.

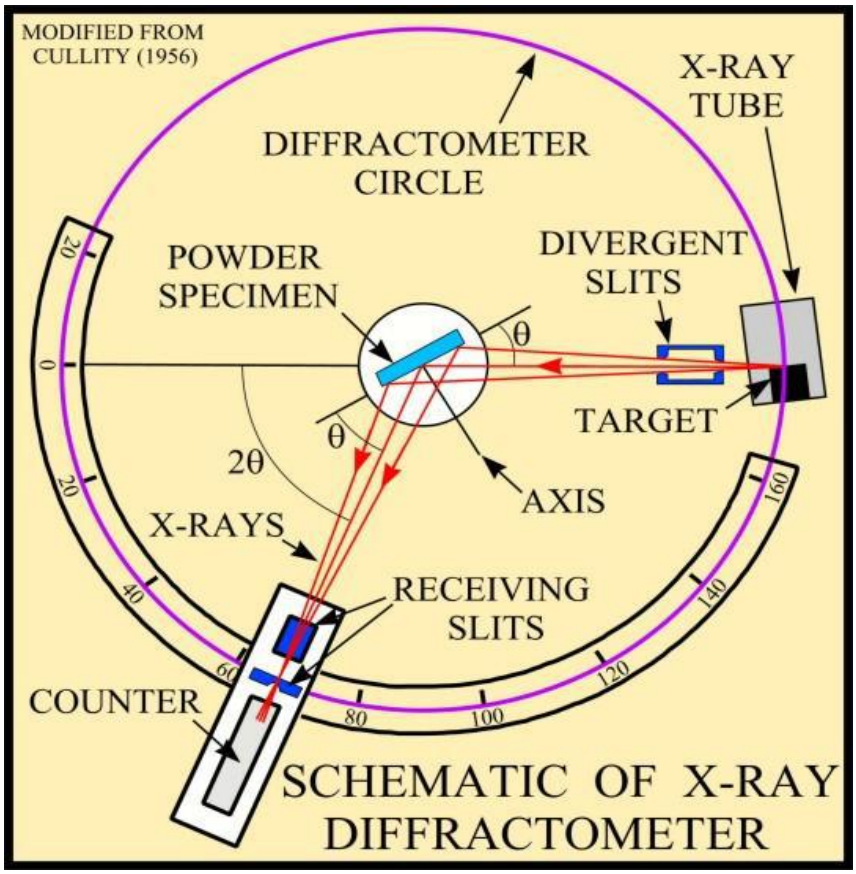

Fig 3.1: Schematic representation of X-ray Diffractometer.

Samples:

The X-ray diffraction is mainly used for "finger print identification" of various solid materials. If normally the sample is ground down to particles of about 0.002mm to 0.005mm cross section. The ideal sample is homogeneous and the crystallites are randomly distributed. The sample is pressed into a sample holder to arrive at a smooth flat surface. In X-ray diffraction, the sample holder is made of aluminium plate.

3.3.2.Applications:

X-ray powder diffraction is most widely used for the identification of unknown crystalline materials (e.g. minerals, inorganic compounds). Determination of unknown solids is critical to studies in geology, environmental science, material science, engineering and biology.

Other applications include:

- Characterization of crystalline materials.
- Identification of fine-grained minerals such as clays and mixed layer clays that are difficult to determine optically.
- Determining Crystallite size for polycrystalline films and materials
- Detecting crystalline minority phases (at concentration greater than 1%).
- Determination of unit cell dimensions.
- Measurement of sample purity.

3.3.3.Strengths of X-Ray Power Diffraction

- Powerful and rapid (< 20 min) technique for identification of an unknown mineral.
- In most cases, it provides an unambiguous mineral determination.
- Minimal sample preparation is required.
- XRD units are widely available.

Fig:3.2 Schematic representation of XRD instrument.

3.4Spectroscopic Analysis:

3.4.1.UV SPECTROSCOPY:

Spectroscopy refers to shining light of a specific color on a sample and observing the absorption, scattering, or other properties of the material under typical conditions. Spectroscopy is a much older, more general technique than scanning probe microscopy and it is offers many complementary insights.

Ultraviolet–visible spectroscopy or ultraviolet-visible spectro-photometry refers to absorption spectroscopy or reflectance spectroscopy in the ultraviolet-visible spectral region. It means that it uses light in visible and adjacent near-UV and near-infrared [NIR] ranges.

Principle of ultraviolet-visible absorption:

UV spectroscopy is a type of absorption spectroscopy in which the light of ultra-violet region (200-400 nm) is absorbed by the molecule. Absorption of the ultra-violet radiations results in the excitation of the electrons from ground state to the higher energy state. The energy of the ultra-violet radiation is absorbed and is equal to the energy difference between the ground state and the higher energy states.

The Molecules containing π-electrons or non-bonding electrons (n-electrons) can absorb the energy in the form of ultraviolet or visible light to excite these electrons to higher anti-bonding molecular orbital. The easier the excited of electrons means that it can absorb only the longer wavelength. Generally, the most favoured transition is formed from the highest occupied molecular orbital (HOMO) to lowest unoccupied molecular orbital (LUMO). For most of the molecules, the lowest energy occupied by the molecular orbitals are s orbital, which corresponds to the sigma bonds. The p orbitals are at somewhat higher energy levels, the orbitals (nonbonding orbitals) with an unshared pair of electrons lie at higher energy levels. The unoccupied or anti-bonding orbitals (and sigma) are the highest energy occupied orbitals. In all the compounds (other than alkanes), the electrons undergo various transitions. Some of the important transitions with increasing energies are: non-bonding to π, non-bonding to s , π to π, s to π and s to s.

UV spectroscopy obeys the Beer-Lambert law, which states that: when a beam of monochromatic light is passed through a solution of an absorbing substance, the rate of decrease in intensity of radiation with the thickness of the absorbing solution is proportional to the incident radiation as well as the concentration of the solution.

The expression of Beer-Lambert law is-

$$\mathbf{A = \log_{1o}(I_0/I) = Ecl.}$$

Where,

A = absorbance

I_0 = intensity of light incident upon sample cell

I = intensity of light leaving sample cell

C = molar concentration of solute

L = length of sample cell (cm)

E = molar absorptivity

From Beer-Lambert law, it is clear that greater the number of molecules capable of absorbing light of a given wavelength, greater is the extent of light absorption. This is the basic principle of UV spectroscopy.

Instrumentation and Working of the UV spectrometers:

Most of the modern UV spectrometers consist of the following parts-

Light Source: Tungsten filament lamps and Hydrogen-Deuterium lamps are most widely used and suitable light source to cover the whole UV region. Tungsten filament lamps are rich in red radiations; more specifically they emit the radiations of 375 nm, while the intensity of Hydrogen-Deuterium lamps falls below 375 nm. Xenon lamps cover a wide spectral range from 320nm to 2200nm range.

Monochromator: Monochromators generally composed of the prisms and slits. Most of the spectrophotometers are the double beam spectrophotometers. The radiation emitted from the primary source is dispersed with the help of the rotating prisms. The various wavelengths of the light source which was separated by the prism are then selected by the slits such that the rotation of the prism results in a series continuously increasing the wavelength to pass through the slits for recording purpose. The beam selected by the slit is monochromatic and further divided into two beams with the help of another prism.

Sample and reference cells: One of the two divided beams is passed through the sample solution (or coated film) and second beam is passed through the reference solution (or the transparent substrate). Both sample and reference solution are contained in the cells. These cells are made of either silica or quartz. Glass can't be used for the cells as it also absorbs light in UV region.

Detector: Generally, there are two photocells serve the purpose of detector in the UV spectroscopy. One of the photocell receives the beam from the sample cell and second detector receives the beam from the reference. The intensity of the radiation from the reference cell is stronger than the beam of sample cell. This results in the generation of pulsating or alternating currents in the photocells.

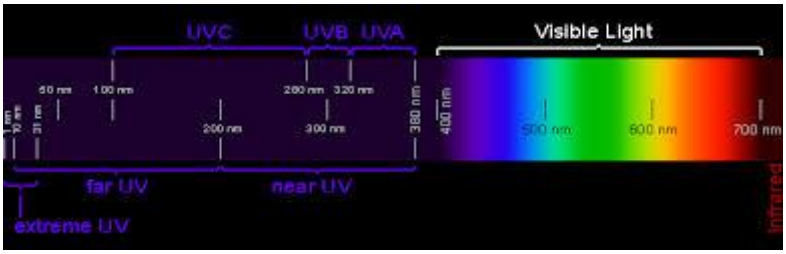

Fig 3.3:Representation of UV visible light

Applications

- **Identification of an unknown compound**- An unknown compound can be identified with the help of UV spectroscopy. The spectrum of unknown compound is compared with the spectrum of a reference compound and if both the spectrums coincide then it confirms the identification of the unknown substance.
- Organic compounds, especially those with have a high degree of conjugation can also absorb light in UV or visible regions of the electromagnetic spectrum, . The solvents for these determinations are often water for water-soluble compounds, or ethanol for organic-soluble compounds. (Organic solvents may have a significant UV absorption, not all solvents are suitable for use in UV spectroscopy. Ethanol absorbs very weak in most wavelengths) Solvent polarity and pH can affect the absorption spectrum of an organic compound.

3.5.Photoluminescence:

Photoluminescence is a light emission from any form of matter after the absorption of photons (electromagnetic radiation). It is one of many forms of luminescence (light emission) and it is initiated by photo excitation (excitation by photons).

Fig 3.4:Schematic representation of Fluorescentsolutions under UV-light

Forms of photoluminescence:

Photoluminescence is an important technique for measuring the purity and crystalline quality of semiconductors, and also for the qualification of the amount of disorder present in a system. Photoluminescence processes can be classified by various parameters such as energy of the exciting photon with respect to the emission. Resonant excitation describes a situation in which photons of a particular wavelength are absorbed and equivalent photons are very rapidly re-emitted. This is often referred to as resonance fluorescence. For materials in

solution or in the gas phase, this process involves electrons but no significant internal energy transitions involving molecular features of the chemical substance between absorption and emission. More processes will occur when a substance undergoes internal energy transitions before re-emitting the energy from the absorption event.

Electrons change energy states by either resonantly gaining energy from absorption of a photon or losing energy by emitting photons. Several variations of photoluminescence exist, including photoluminescence excitation (PLE) spectroscopy.

Time-resolved photoluminescence (TRPL) is a method where the sample is excited with a light pulse and then, the decay in photoluminescence with respect to time is measured. This technique is useful for measuring the minority carrier lifetime of the phosphor under study.

3.6.Fourier transform infrared spectroscopy [FTIR]:

FT-IR stands for Fourier Transform Infrared, the preferred method of infrared spectroscopy. In infrared spectroscopy, IR radiation is passed through a sample. Some of the infrared radiation is absorbed by the sample and some of it is passes through (transmitted). The resulting spectrum represents the molecular absorption and transmission, creating a molecular fingerprint of the sample. Like a fingerprint no two unique molecular structures produce the same infrared spectrum. This makes infrared spectroscopy useful for several types of analysis.

Fourier transform infrared spectroscopy (FTIR) is a technique which is used to obtain an infrared spectrum of absorption or emission of a solid, liquid or gas. An FTIR spectrometer simultaneously collects high spectral resolution data over a wide spectral range. This confers a significant advantage over a dispersive spectrometer which measures intensity over a narrow range of wavelengths at a time. The term Fourier transform infrared spectroscopy originates from the fact that a Fourier transform (a mathematical process) is required to convert the raw data into the actual spectrum.

Conceptual introduction:

Fourier Transform Infrared (FTIR) Spectroscopy was first developed by astronomers in the early 1950s to study the infrared spectra of distant stars has now been developed into a very powerful technique for the detection of very weak signals from the environmental noise. It is a simple mathematical technique to resolve a complex wave into its frequency components. The conventional IR spectrometers are not of much use for the far IR region (20-400 cm^{-1}) as the sources are weak and detectors are insensitive. FTIR has made this energy limited region more accessible. It has made the middle infrared (400-4000 cm^{-1}) also more useful.

Fourier Transform Infrared (FT-IR) spectrometry was developed in order to overcome the limitations encountered with dispersive instruments. The main difficulty was the slow scanning process. A method for measuring all the infrared frequencies simultaneously, rather than individually was needed. A solution was developed which employed a very simple optical device called interferometer. The interferometer produces a unique type of signal which has all the infrared frequencies "encoded" into it. The signal can be measured very quickly, usually in the order of one second or so. Thus, the time element per sample is reduced to a matter of a few seconds rather than several minutes.

An FTIR interferogram: The central peak is at the ZPD position ("Zero Path Difference" or zero retardation) where the maximum amount of light passes through the interferometer to the detector. The goal of any absorption spectroscopy (FTIR, ultraviolet-visible ("UV-Vis") spectroscopy, etc.) is to measure, how well a sample absorbs light at each wavelength. The most straightforward way to do this is the "dispersive spectroscopy" technique, is to shine a monochromatic light beam at a sample, to measure how much of the light is absorbed, and repeat for each different wavelength.

Developmental background:

The first low-cost spectrophotometer is capable of recording an infrared spectrum was the Perkin-Elmer Infrared produced in 1957. This instrument covered the wavelength range from 2.5 μm to 15 μm (wavenumber range 4000 cm^{-1} to 660 cm^{-1}). The lower wavelength limit was chosen to encompass the highest known vibration frequency due to a fundamental molecular vibration. The upper limit was imposed by the fact that the dispersing element was a prism made from a single crystal of rock-salt (sodium chloride) which becomes opaque at wavelengths longer than about 15 μm; this spectral region became known as the rock-salt region. Later instruments used potassium bromide prisms to extend the range to 25 μm (400

cm^{-1}) and caesium iodide 50 μm (200 cm^{-1}). The region beyond 50 μm (200 cm^{-1}) became known as the far-infrared region; at very long wavelengths it merges into the microwave region. Most interferometers employ abeam splitterwhich takes the incoming infrared beam and divides it into two optical beams. One beam reflects off of a flat mirror which is fixed in place. The other beam reflects off of a flat mirror which is on a mechanism which allows this mirror to move a very short distance (typically a few millimetres) away from the beam splitter.

The two beams reflect off their respective mirrors and are recombined when they meet back at the beam splitter. Because the path that one beam travels is a fixed length and the other is constantly changing as its mirror moves, the signal which exits in the interferometer is the result of these two beams "interfering" with each other. The resulting signal is called an interferogram which has the unique property that every data point (a function of the moving mirror position) which makes up the signal has information about every infrared frequency which comes from the source. This means that as the interferogram is measured, all frequencies are being measured Simultaneously. Thus, the use of the interferometer results in extremely fast measurements.

3.6.1 Advantages of FT-IR:

Some of the major advantages of FT-IR over the dispersive technique include:

- FT-IR is highly sensitive and quick method to achieve high quality spectrum.
- This spectroscopy gives better signal to noise ratio compared to dispersive instrument.
- With FT-IR spectrum can be obtained very quickly and saves time
- Gases, solid as well as liquid can be analysed with FT-IR.
- By using FT-IR no external calibration is required and gives accurate results.
- FT-IR is non-destructive technique.
- Organic compounds and inorganic compounds can be identified easily using Fourier transform infrared spectroscopy.
- FT-IR can identify even small concentration of contaminants.
- FT-IR has a laser beam which keeps the FT-IR instrument accurately calibrated.

- It generally completes a scans within one to two seconds.
- High resolution.

3.6.2 Disadvantages oF FT-IR:

- FT-IR instrument have only single beam while, dispersive instrument general have a double beam.
- Environmental conditions around the FT-IR instrument can cause variations in the spectra, hence background scans and multiple scans of the same sample are required.
- Complex samples like mixtures of bacteria produce overlapping spectra, which may lead to misinterpretation of results. Hence a bacterial separation or purification step is required in some instances.

3.6 Jablonski Diagram

A Jablonski diagram is a diagram that illustrates the electronic states of a molecule and the transitions between them. The states are arranged vertically by energy and grouped horizontally by spin multiplicity. Non radiative transitions are indicated by squiggly arrows and radiative transitions by straight arrows. The vibrational ground states of each electronic state are indicated with thick lines, the higher vibrational states with thinner lines. The diagram is named after the Polish physicist Aleksander Jabłoński.

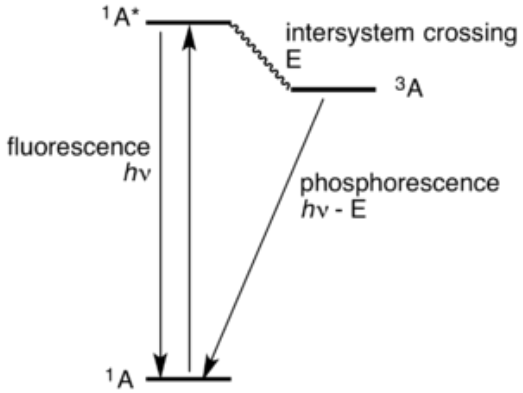

Fig 3.5:Jablonski diagram showing the excitation of molecule A to its singlet excited state ($^1A^*$)

Transitions

Radiative transitions involve the absorption, if the transition occurs to a higher energy level, or the emission, in the reverse case, of a photon. Non radiative transitions arise through several different mechanisms, all differently labeled in the diagram. Relaxation of the excited state to its lowest vibrational level is called Vibrational relaxation. This process involves the dissipation of energy from the molecule to its surroundings, and thus it cannot occur for isolated molecules. A second type of nonradioactive transition is internal conversion (IC), which occurs when a vibrational state of an electronically excited state can couple to a vibrational state of a lower electronic state. A third type is intersystem crossing (ISC), this is a transition to a state with a different spin multiplicity. In molecules with large spin-orbit coupling, intersystem crossing is much more important than in molecules that exhibit only small spin-orbit coupling.

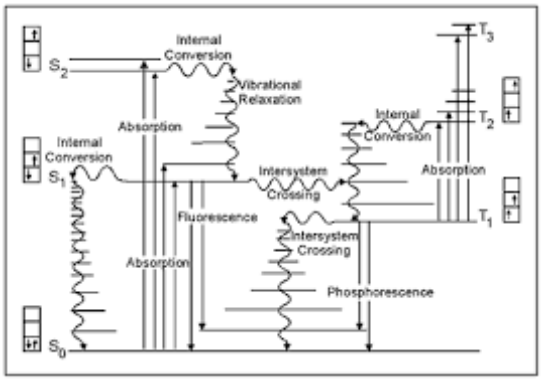

Fig 3.6: Schematic Representation of Jablonski diagram

3.7 References:

1) http://www.eag.com/mc/x-ray-diffraction.html
2) S.J. Limmer , S.Vince Cruz and G.Z.Cao; Advanced Material; 2003
3) http://www.intertek.com/analysis/microscopy/edx/
4) Moore, D. M. and R. C. Reynolds, Jr. 1997. X-Ray diffraction and the identification and analysis of clay minerals. 2nd Edition. Oxford University Press, New York
5) Cullity, B. D. 1978. Elements of X-ray diffraction. 2nd edition. Addison-Wesley, Reading, Mass.
6) Klug, H. P., and L. E. Alexander. 1974.X-ray diffraction procedures for polycrystalline and amorphous materials. 2nd edition.Wiley, New York.
7) Griffiths, P.; de Hasseth, J.A. (18 May 2007). Fourier Transform Infrared Spectrometry (2nd edition.). Wiley-Blackwell.
8) Joseph Goldstein (2003). Scanning Electron Microscopy and X-Ray Microanalysis. Springer. Retrieved 26 May 2012.
9) Jabłonski, Aleksander "Efficiency of Anti-Stokes Fluorescence in Dyes" Nature 1933, volume 131, pp. 839-840.

RESULTS AND DISCUSSION

CHAPTER IV

RESULTS AND DISCUSSION

4.1 Introduction

This chapter deals with the results of Sn_2Sb_3 and dysprosium doped $Sn_{2-x}Dy_xSb_3$. Out of the various compositions where x= 0.2, 0.4 and 0.6, x=0.6 resulted in better results and hence x=0.6 is presented here.

4.2 Structural Characterization

4.2.1 X-Ray Diffraction Analysis (XRD)

The prepared Sn_2Sb_3 and $Sn_{1.4}Dy_{0.6}Sb_3$ composition doped with dysprosium is investigated with X-ray Diffraction to determine the phase formation. The X-Ray diffraction pattern of Sn_2Sb_3 doped with dysprosium compositions as prepared by co-precipitation method is shown in Figure 4.1. The Sn_2Sb_3 in the composition 2:3 is doped with three compositions namely 0.2, 0.4 and 0.6 of dy in this host lattice. The results observed for 0.6 is the best and only this composition results are presented here. In all the samples, the peaks at 28^0,41^0,42^0,51^0 and 60^0 corresponds to the (101), (012), (110), (003), and (202) for Sn_2Sb_3.

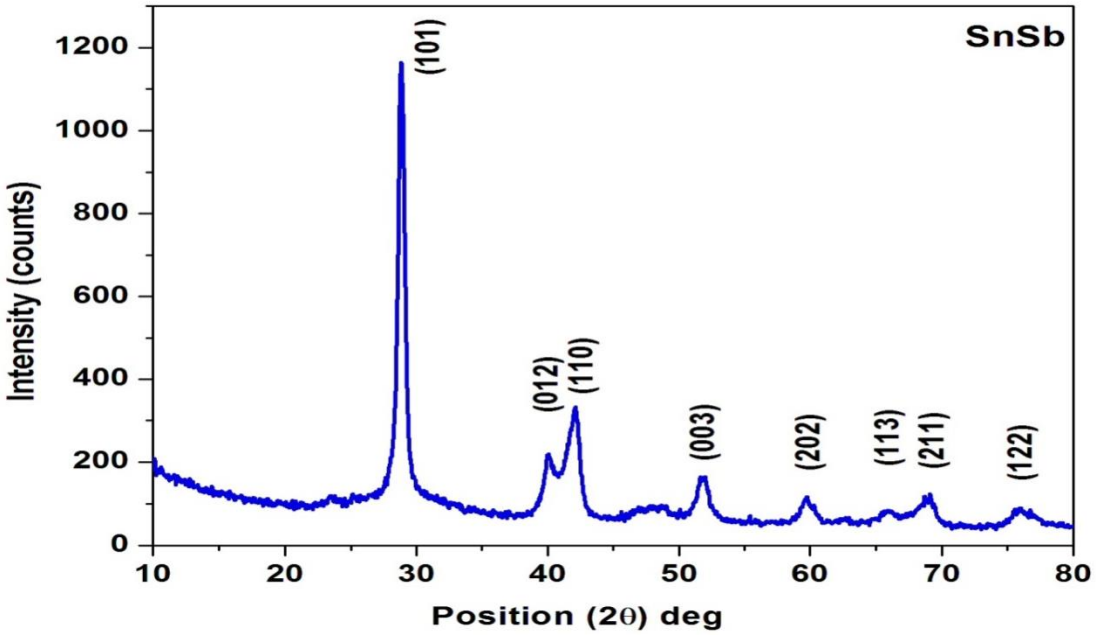

Figure 4.1 X-ray Diffractogram of the Sn_2Sb_3 alloy

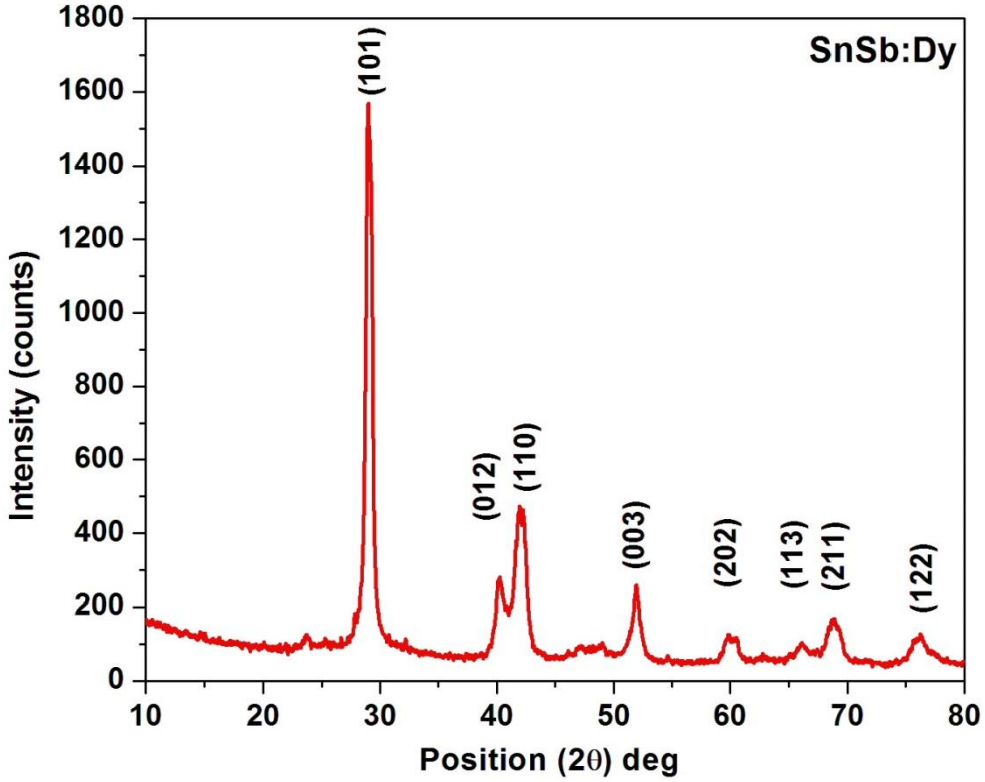

Figure 4.2. X-ray diffractogram of the $Sn_{1.4}Dy_{0.6}Sb_3$

A sharp peak obtained in XRD pattern indicates the crystallinity of the prepared samples.The XRD pattern observed for $Sn_{1.4}Dy_{0.6}Sb_3$ is notdifferent from that of the Sn_2Sb_3. This indicates that the structure is left undisturbed by the dysprosium atoms in the substitution limits which are chosen in these studies. It is also to be noted that there are no new peaks observed in doped sample which is an indication of the stable crystal structure for the doped Sn_2Sb_3. The results are analyzed with the standard diffraction pattern (JCPDS card no- 33-0118) and the crystal system possessesrhombohedral structure. Due to the fact that all the peaks except one at 68˚ which is assigned as (004) peak falls into the formula –h+k+l=3n which is for a hexagonal structure. Hence the structure has got rhombohedral structure falling into irregular hexagonal distribution of atoms. The lattice parameter calculated is given in the Table 1. Compared to the JCPDS lattice parameters, there is a size reduction in "c" when "a" is maintained and when "a" is reduced "c" is blotted. But, it is to be noted that this size variation is just few 100^{th} is an angstrom and is not of much importance. The similar behavior is observed for the$Sn_{1.4}Dy_{0.6}Sb_3$. All the remaining peaks are assigned to the corresponding (hkl) planes based on the JCPDS data as indicated in the figure 4.1 and 4.2 respectively.

Crystallite size is calculated by using Debye Scherrer formula

$d = 0.9\lambda / \beta \cos(\theta)$

where,

d is the Crystallite size,

λ is the wavelength of the radiation (1.5405Å for Cu-Kα radiation),

β is the full width at half maximum of the peak (radians),

θ is half of the peak position (radians).

The diffraction peaks observed at 28.75^0, 40.04^0, 41.11^0, 51.87^0, 59.64^0, 66.01^0, and 68.95^0 shows a small shift in position towards the higher angle side in the doped sample compared to the undoped sample which is an indication of either the crystallite size increment and increased strain in the $Sn_{1.4}Dy_{0.6}Sb_3$. Lattice strain value of both the samples were calculated using the formula,

$$\varepsilon = \beta \cot(\theta)$$

where

ε - Strain

β- Full width at half maximum of the peak (radians)

θ- half of the peak position

The calculated values of crystallite size, lattice strain and all the other lattice parameters obtained for both the samples are listed in the Table 4.2. The increment in crystallite size is observed for $Sn_{1.4}Dy_{0.6}Sb_3$sample from 16 nm to 26 nm. This may be due to the higher ionic radius of dysprosium. (Dy: 0.912Å) $Sn_{2-x}Dy_xSb_3$. (Sn: $0.55A^0$, Sb: $0.76A^0$)

Table 4.1 The different <hkl> planes assignment to the XRD peaks obtained Sn_2Sb_3; lattice constants, a= 4.428Å, c= 5.2886Å, Volume = 89.797Å^3

No .of peaks	2θ (deg)	h	K	l	$1/d^2$ cal ($x10^8$)	FWHM	Strain
1	23.626	1	0	1	2.451	0.802	0.167
2	28.757	0	1	2	2.105	0.334	0.005
3	40.042	1	1	0	3.181	0.401	0.007
4	42.110	0	0	3	1.320	0.267	0.004
5	51.871	2	0	2	1.140	0.669	0.011
6	59.646	1	1	3	1.179	0.802	0.014
7	66.010	2	1	1	1.028	0.802	0.014
8	68.959	1	2	2	2.451	0.936	0.016

Table 4.2 The different <hkl> planes assignment to the XRD peaks obtained $Sn_{1.4}Dy_{0.6}Sb_3$; lattice constants, a=4.3895 Å, c= 5.289Å, Volume = 88.137Å^3

Peak no	2θ	h	K	L	Calculated ($1/d^2$)	FWHM	Strain
1	28.929	1	0	1	0.1051	0.2676	0.0690
2	40.115	1	1	0	0.1985	0.2676	0.0976
3	41.914	0	0	3	0.2155	0.4684	0.1793
4	51.935	2	0	2	0.3281	0.3346	0.0976
5	59.746	1	1	3	0.4182	0.4015	0.2314
6	66.140	2	1	1	0.5020	0.6691	0.4356

The lattice parameter of the undoped and doped are almost same indicating that the distortion in the lattice is very minimal. However the local strain caused due to the local environment is extremely high at specific planes especially at 211 plane.

4.3 Optical structure analysis

4.3.1 Fourier Transform Infrared Spectroscopy:

In the present work, the characteristic vibrational frequencies of Sn_2Sb_3 and that of $Sn_{2-x}Dy_xSb_3$are compared.FTIR spectra of$Sn_{2-x}Dy_xSb_3$are recorded at room temperature in the wavelength range of 4000- 400 cm^{-1}. The range of vibrations obtained in the region of 3500-4000 cm^{-1} are attributed to the OH vibrations which may be due to the moisture content arose from the hygroscopic nature of KBr during the pelletization. Hence the spectra are presented only upto 3500cm^{-1}.$Sn_{1.4}Dy_{0.6}Sb_3$. Comparing the FTIR spectrum obtained for metal oxide nanoparticles, it can be claimed that pristine and doped SnSb samples are free from oxide impurities. As none of these peaks are observed and hence it is assured that the alloys are devoid of oxygen in the lattice. The obtained vibrational peaks and the corresponding shift in wavenumbers for doped Sn_2Sb_3 are listed in the Table 4.1. In the dysprosium substituted sample, there is severe vibration at small amplitudes from 2100 to 3400cm^{-1}. The suspicion of instrumental error is ruled out as the pure sample has shown better results in this region. Hence, it is concluded that this oscillation may be due to the weak bonding of Dy and thus causing lattice loosening in the sample.

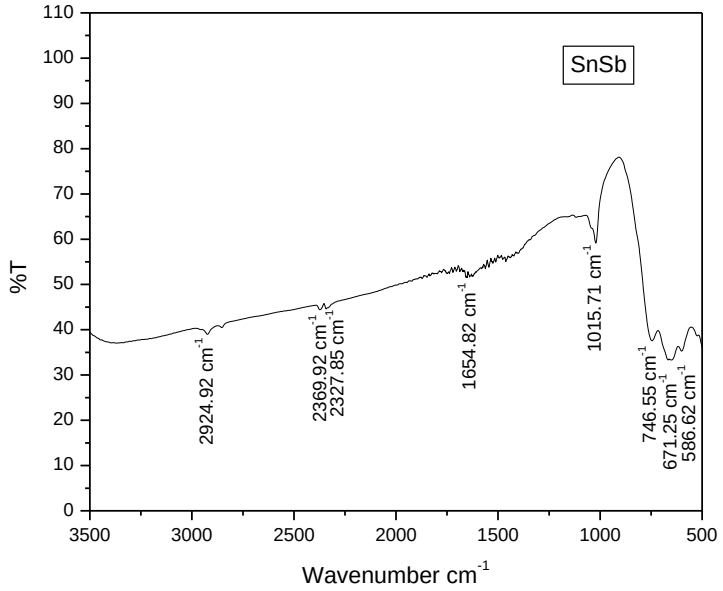

Figure 4.3 FTIR Spectrum of Sn_2Sb_3

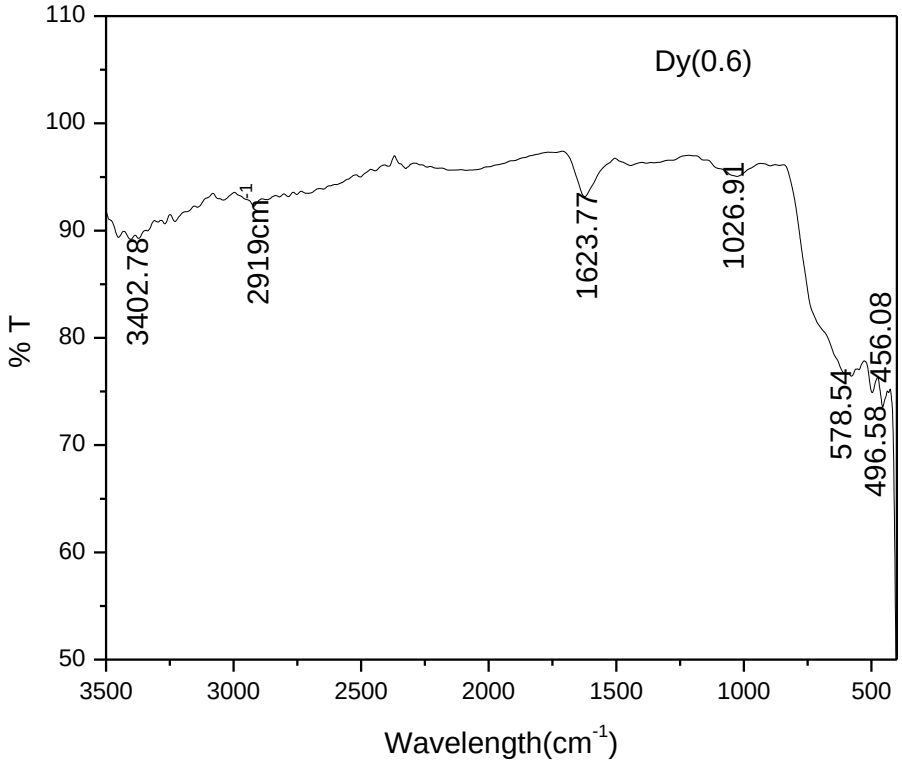

Figure 4.4 FTIR Spectrum of $Sn_{2-x}dy_xSb_3$

Table 4.3 The vibrational peaks & the corresponding shift wave number for doped of Sn_2Sb_3

Peak no	SnSb	SnSb: Dy	Peak
1	-	456.08	After addition of Dy
2	-	496.58	
3	586.62	578.54	Sn-Sb
4	671.25	-	Disappeared after addition of Dy
5	746.55	-	
6	1015.71	1026.91	Sn-Sb
7	1654.82	1623.77	OH vibration
8	2327.85	-	Sn-Sb
9	2369.82	-	
10	2924.92	2919.70	Impurities from acetone
11	-	3402.78	OH vibration

Comparing both the FTIR spectra, there is a slight shifting towards higher wavenumber which shows that bond has altered after the addition of dopants into the pure Sn_2Sb_3. New peaks indicate that the Dy-Sn or Dy-Sb bond occurs in the structure. Altogether, it is clear that Dy has entered into the crystal structure and bonded with Sn/Sb. However, the rhombohedral structure is unaltered and this statement is validated on comparison with the XRD pattern observed for both the samples.

4.4 Optical Absorption studies:

Uv Vis NIR Spectrophotometer is employed to understand the absorption profile of these samples. The absorption spectrum is obtained from 200nm to 2200nm using Jasco V600 instruments.

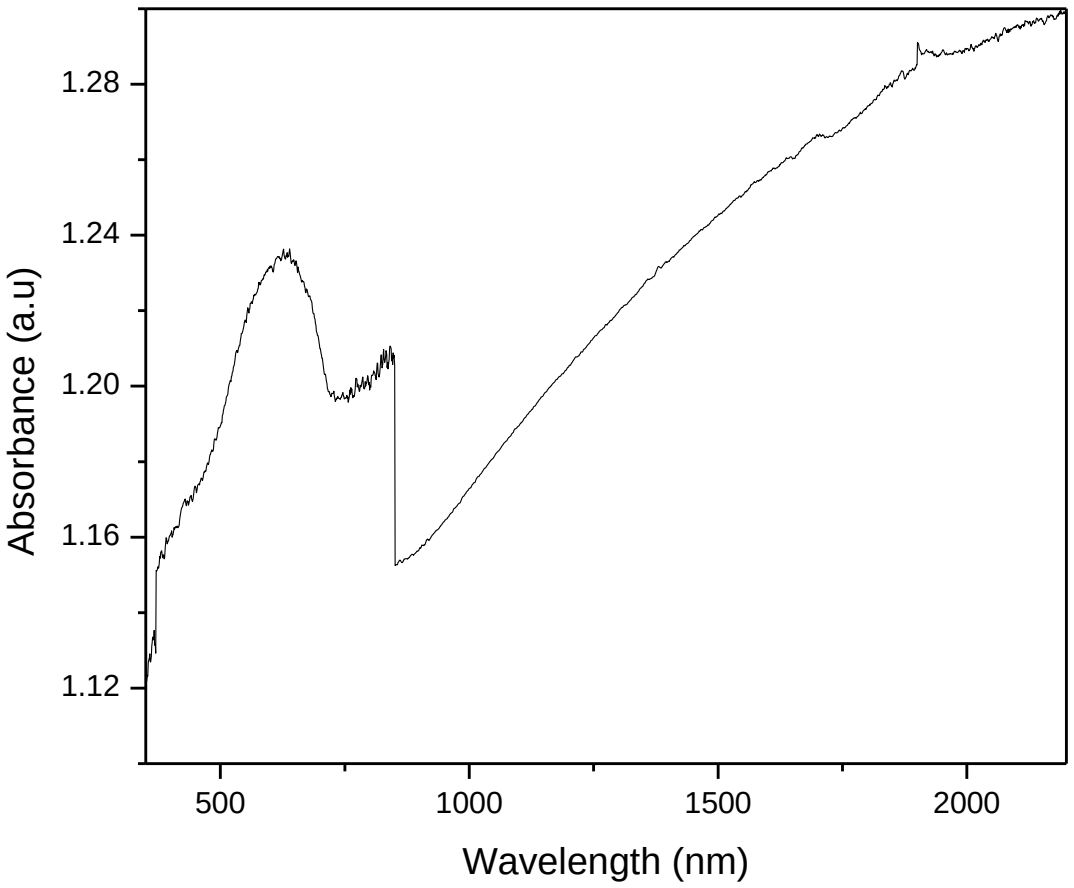

Figure 4.5 Absorbance spectrum sample$Sn_{2-x}Dy_xSb_3$

Transmittance spectrum is also acquired and the tauc plot with $(\alpha h\nu)^2$ Vs $h\nu$ is plotted. The plot is shown in figure 4.6

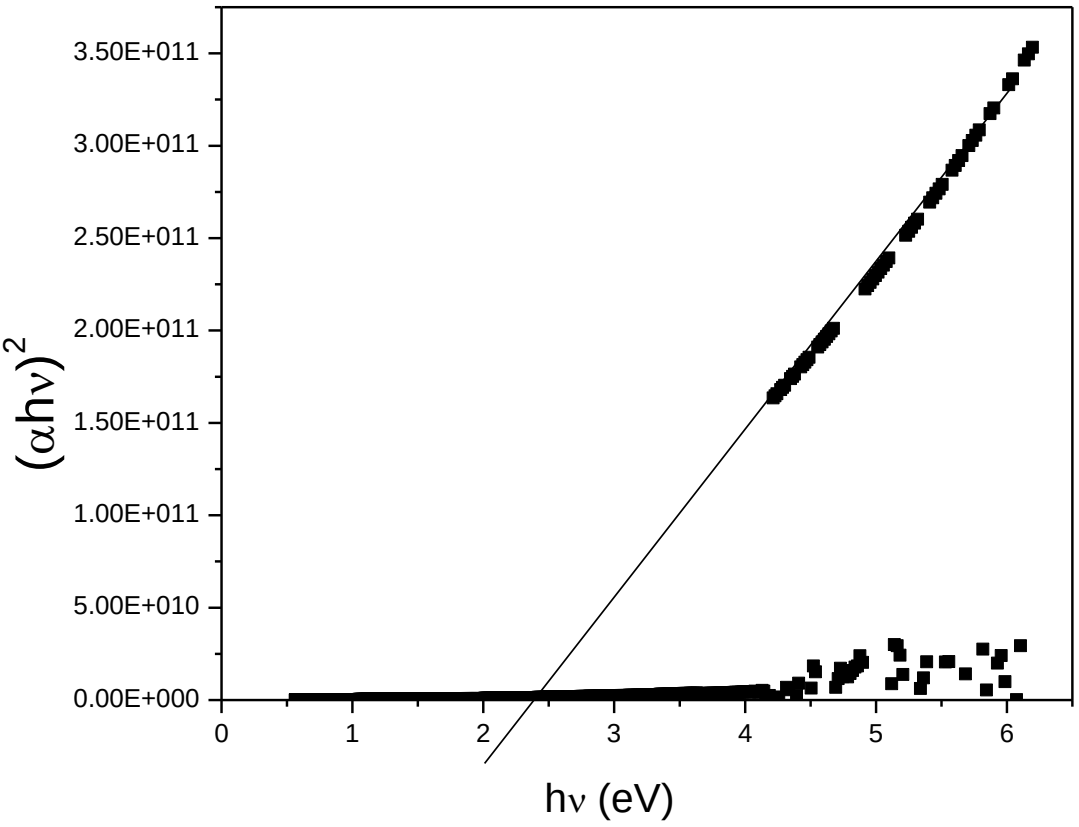

Figure 4.6. Tauc plot of $Sn_{2-x}Dy_xSb_3$showing the discontinuity in the energy levels

The energy gap of 2.48eV is observed for the$Sn_{2-x}Dy_xSb_3$.Further analysis in lower energy side shows interesting effects due to the substitution of dysprosiumin the lattice which has not been observed in the Sn_2Sb_3sample.

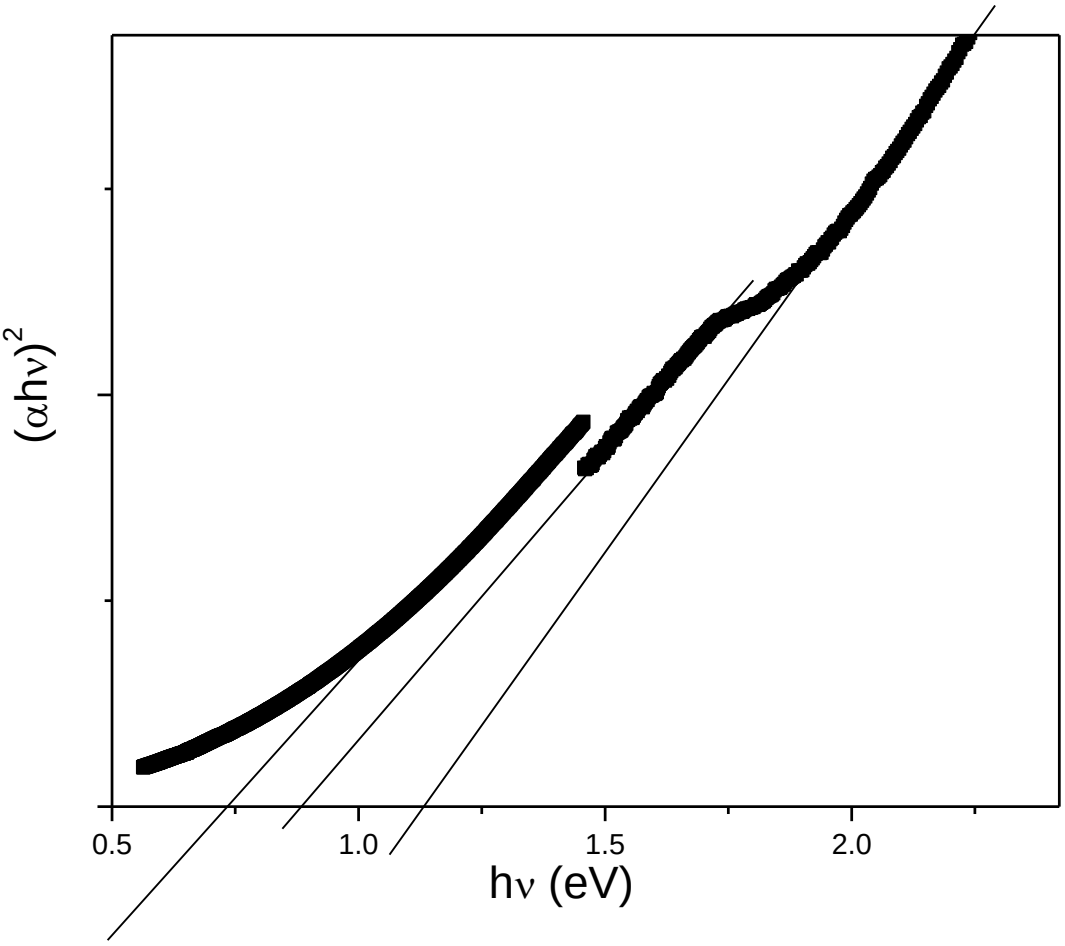

Fig 4.7The discontinuity at deep level of energy observed in the $Sn_{2-x}Dy_xSb_3$ sample

This shows another discontinuity with a band gap of 1.13 eV originally due to the host of Sn_2Sb_3 that has been reduced due to the occupation of dysprosium which reduced the forbidden gap to 0.88eV. A typical strain is also observed due to the mismatch between the Sn_2Sb_3 lattice and dysprosium atoms. For reference, the energy band diagram of E vs k for both free electron and in a crystal lattice is shown here in Figure 4.8. Consolidated band structure is shown in Figure 4.10. Hence it is understood that there is a ground level S_0 and a band S_1 and S_2 are present. The effect of generated energy levels due to doping is seen between S_0 and S_1 bands very clearly. Thus the electronic band structure of the $Sn_{2-x}Dy_xSb_3$ is clearly studied. Further analysis is made for the emission studies using photoluminescence studies.

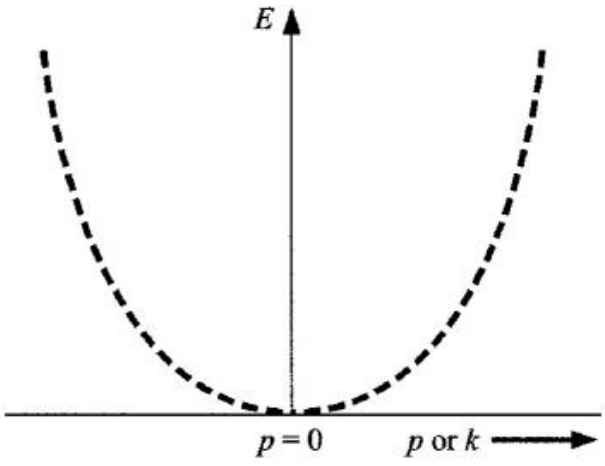

Figure 4.8E Vs k diagram for free particle with continuous energy levels

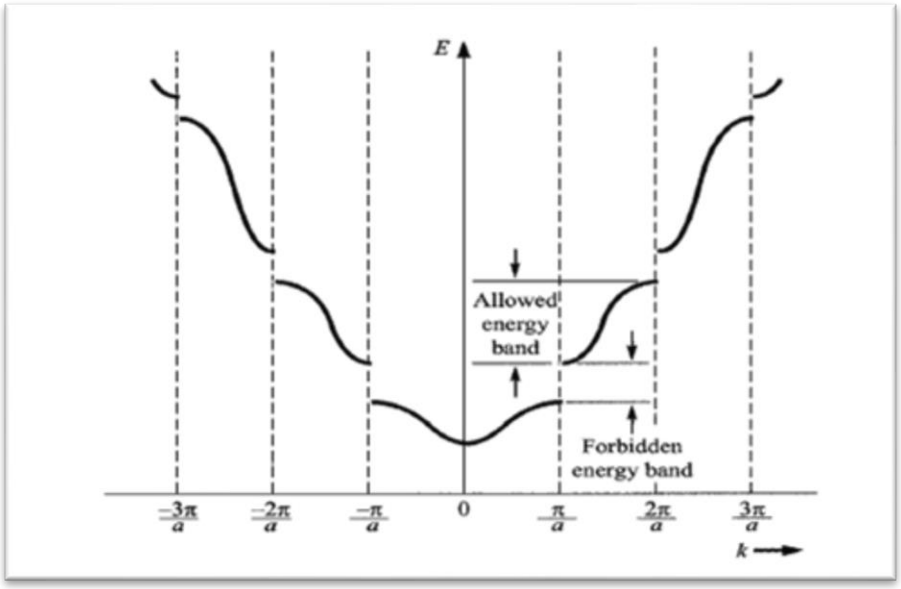

Figure 4.9 E Vs k diagram for crystal lattice with discontinuous energy levels

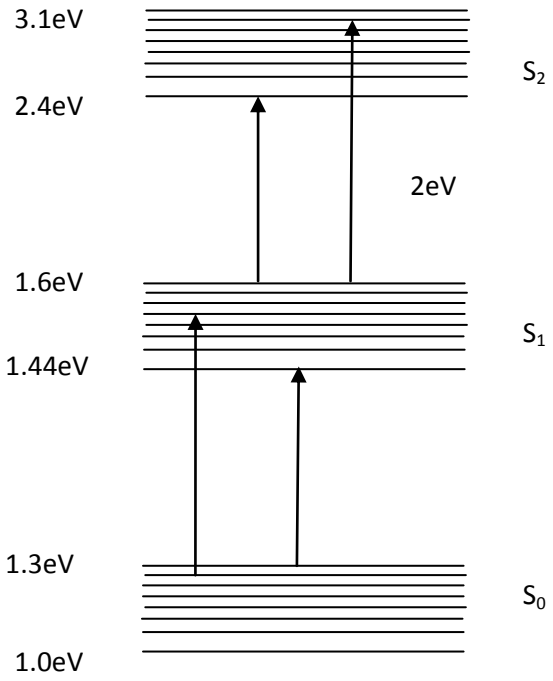

Figure 4.10 Energy band structure as inferred from the tauc plot

Photoluminescence (PL) studies:

PL is studied for all the compositions but the transition for 0.6 composition has shown a difference in the tauc plot and hence the composition 0.6 alone is discussed here. The PL excitation of Sn_2Sb_3 sample at 340nm excitation is shown for reference in Figure 4.8. The dysprosium substitution has made a broad emission from 400 nm to 650 nm when compared to the undoped. Thus a variation in emission profile that is favourable for any application in lighting is observed in this sample. For the convenience of the reader, the absorption and PL is plotted a 340nm excitation together. There exists a broad overlap with the absorption and emission over the visible range. Any further texturing of the material or size selective operation of the material may result in the prospective lighting application material.

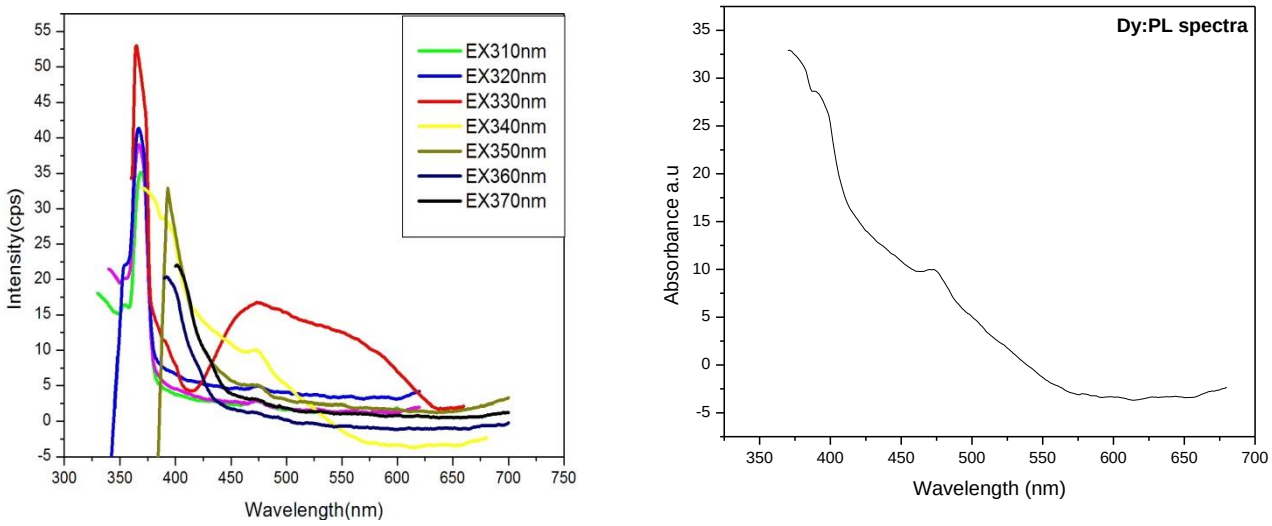

Figure 4.11(a)PL emission of $Sn_{2-x}Dy_xSb_3$ at different excitation wavelengths.

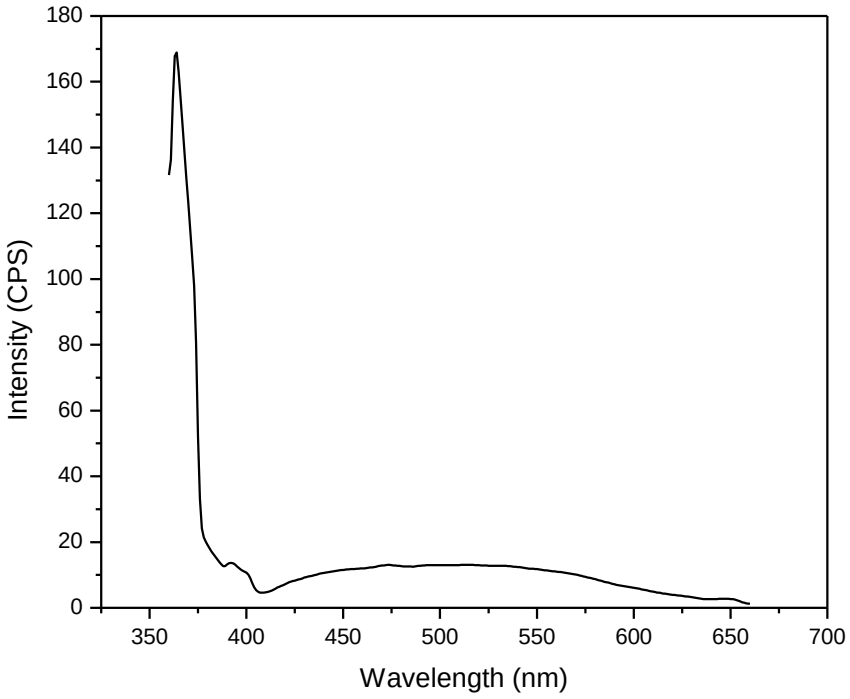

Figure 4.11(b) PL emission of Sn_2Sb_3 at excitation at 340 nm

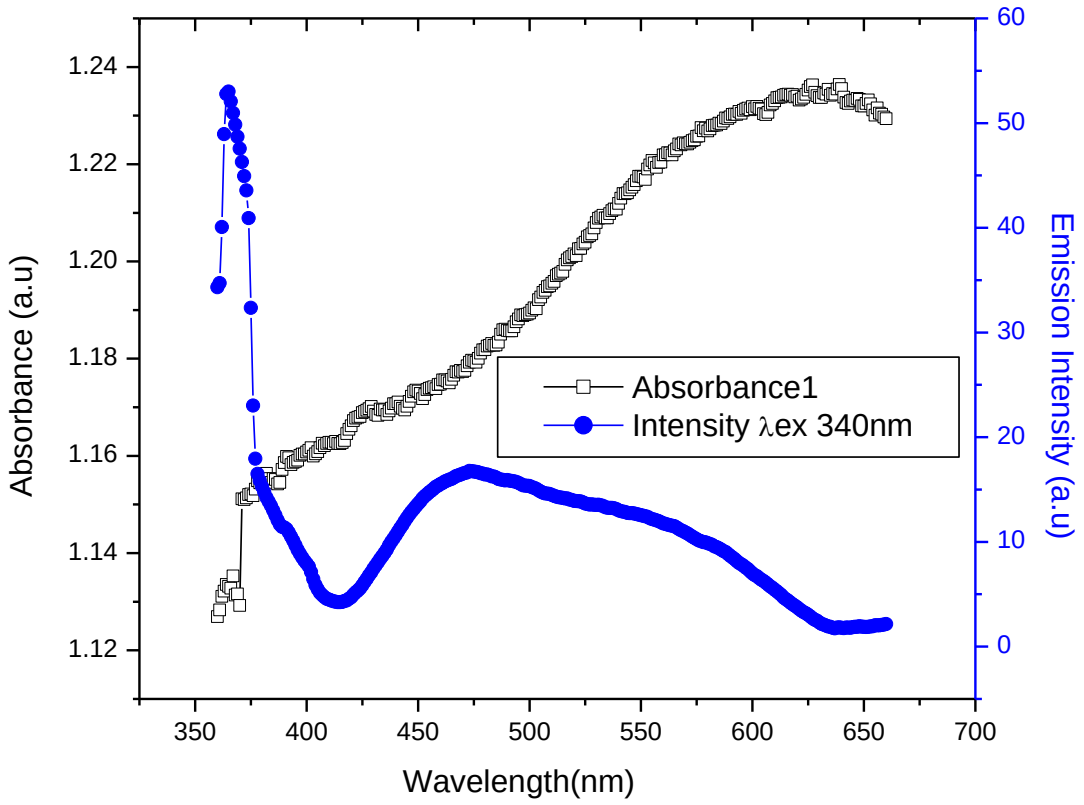

Figure 4.12 Absorbance and PL emission with λex at 340nm

4.5 References

1) Vicente Scanchez Escribano, Enrique Fernandez Lopez, Marta Panizza, Carlo Resini, Jose Manuel Gallardo Amores, Guido Busca, Characterization of SnSb powders by X-ray diffraction and Vibrational and Electronic Spectroscopy, Solid State Sciences, Volume-5 (10), (2003), pp 1369-1376.

2)J. Kaspar, P. Fornasiero, G.Balducci, R. Di Monte, N. Hickey, V. Sergo, Efect of SnSb content on textural and structural properties of solid solutions made by citrate complexation route, Inorganica Chimica Acta, Volume- 349, (2003), pp 217-226.

3)Enrique Fernandez Lopez, Vicente Scanchez Escribano, Marta Panizza, Maria M. Carnasciali, Guido Buca, Vibrational and Electronic Spectroscopic properties of SnSb powders, Journal of Material Chemistry, Volume-11, (2001), 1891-1897.

4)P. Fornasiero, J. Kaspar, M. Graziani, Redox Behavior of High Surface Area,Mixed Oxide, Journal of Catalysis, Volume-167, (1997), pp 576-580.

5) A.Lamacz, M.Pawlyta, L.A.Dobrzanski, A.Krzton, Archieves of Materials Science and Engineering, Volume-48 (2), (2011), pp 89-96.

6) P. Nithyadharseni, B. Nalini, P. Saravanan, Applied Surface Science 311 (2014) 503–507

7).Laszlo Korosi, Szilvia Papp, Imre Dekany, Thin Solid Films 519 (2011) 3113–3118

8)YANG Fen, ZHANG Xue-jun, WU Xu, TIAN Fang, GAN Fu-xing, Trans. Nonferrous Met. Soc. China 17(2007)

SUMMARY AND CONCLUSION

CHAPTER-V

SUMMARY AND CONCLUSION

5.1 Conclusion

Sn_2Sb_3 and $Sn_{2-x}Dy_xS_3$ are prepared with coprecipitation method. The prepared powders had a single phase with rhombohedral structure that is confirmed by X-Ray diffractometry. The oxide formation is ruled out using the FTIR analysis. Also the FTIR analysis ensures the entry of Dysprosium in the SnSb lattice. The electronic structure is studied using UV-Vis-NIR spectrophotometer and Spectrofluorimeter. The absorption is very appealing as it spans in the visible region and extends to the IR region also. The emission is also prospective as it has a broad emission over the visible region when excited at 340nm. The influence of dysprosium in the lattice is well seen with the tauc plot where forbidden gap is filled with allowed energy levels after the substitution.

.